

**Detection and attribution of carbon cycle processes from  
atmospheric O<sub>2</sub> and CO<sub>2</sub> observations at Baring Head,  
New Zealand**

**By Thomas Barningham**

**Student No: 100033296**

Thesis presented in part-fulfilment of the degree of Master of Science in accordance with the regulations of the University of East Anglia.

School of Environmental Sciences

University of East Anglia

Norwich Research Park

Norwich

NR4 7TJ

© 2013 Thomas Barningham

This copy of the dissertation has been supplied on condition that anyone who consults it is understood to recognise that its copyright rests with the author and that no quotation from the dissertation, nor any information derived there from, may be published without the author's prior written consent. Moreover, it is supplied on the understanding that it represents an internal University document and that neither the University nor the author are responsible for the factual or interpretative correctness of the dissertation.

## Acknowledgements

First and foremost I would like to thank my supervisor, Andrew Manning, for his continuous support and advice throughout the preparation of thesis. We spent many hours in his office discussing various ideas and topics related to this project. I found this one-to-one teaching time extremely valuable and came away from many meetings feeling more inspired (or reassured!) about the analysis I was doing. Andrew also gave up a lot of his own time to adapt the Weybourne IDL routine to the Baring Head dataset to produce the plots that I used to identify the carbon cycle events in this study. Given that my own programming knowledge is very elementary, adapting the routine myself would not have been possible within the time frame of the project and so I'm very grateful to Andrew for persevering with this often frustrating task. In adapting the routine, Andrew continuously kept me in the loop as to how the routine was being adapted, and through this gave me a "crash-course" in IDL programming that I hope to build upon through my Ph.D research.

Secondly, I would like to thank Penelope Pickers, Andrew's current first year PhD student for her help with running curve-fitting routines to my data. Penelope was in the same position as me last year, completing her Master's thesis, entitled "Investigating bias in the application of three curve fitting programs to atmospheric time series". She is therefore an expert on running these procedures and taught me the meaning of the various aspects of the Fortran Hpspline routine and kindly ran the data for me.

I would also like to thank Rachel Corran, the first year research assistant who joined Andrew's research group during the summer in order for her to gain valuable experience within active areas of environmental research. Rachel assisted me in producing many of the Hysplit trajectories (under my instruction) for the events that I identified. Running each trajectory analysis was a time-consuming, repetitive process and delegating this task to her allowed me to focus more time on the other areas of my analysis. Rachel also had the tedious task of "cleaning up" the Baring Head data set. This involved visually looking through the O<sub>2</sub>, CO<sub>2</sub> and APO datasets to identify and remove erroneous data points. This "clean-up" of the data was essential in avoiding poor curve-fits in the Hpspline curve-fitting procedure and also contributed to a better presentation of the Baring Head dataset.

Last but not least, I would like to thank both Gordon Brailsford (NIWA, NZ) and Britt Stephens (NIWA, NZ and NCAR, USA) for their years of work collecting the Baring Head O<sub>2</sub> and CO<sub>2</sub> measurements, carrying out the exhaustive data processing, and making the datasets available to me.

## Abstract

The aim of my thesis project was to investigate the variability of atmospheric O<sub>2</sub> and CO<sub>2</sub> observations made at Baring Head, New Zealand, for the period 1999-2012, to make deductions on the temporal and spatial variability of the Southern Ocean carbon cycle. This was achieved through the identification of the carbon cycle processes of marine NPP and ventilation of deep CO<sub>2</sub>-rich, O<sub>2</sub> deficient water masses in the derived atmospheric APO observations, defined as “events”. A total of 52 NPP and 26 ventilation events were identified in the data set. These were found to accurately depict the seasonal cycle of APO at BHD, but not the inter-annual variability. Additionally, inter-annual variability of APO observations could not be explained by the SAM and ENSO climate indices. The difference in the mean APO recorded by the events was found to be significantly different ( $P = 0.001$ ;  $<0.01$ ) between the autumn and spring months, further confirming the capture of the APO seasonal cycle in the identified events. Furthermore, the events were characterised by the rate of APO change over the duration of the event. NPP events showed  $\Delta\text{APO}/t$  values of  $\sim 2\text{-}3$  per  $\text{meg hr}^{-1}$  compared to ventilation events which typically displayed  $\Delta\text{APO}/t$  values of  $<1$  per  $\text{meg hr}^{-1}$ . This was interpreted to reflect the different spatial scales that these events occur over. A common APO exchange ratio for the carbon cycle was suggested from the data, but not firmly ascertained due the paucity of sample points. A simple conceptual model of air-sea gas exchange was constructed to reconcile satellite NPP and pO<sub>2</sub> concentrations at the MLD with the atmospheric APO observations. The model consistently overestimated both the NPP and magnitude of O<sub>2</sub> change resulting from ventilation compared to satellite NPP and pO<sub>2</sub> concentrations at the MLD. The limitations of the parameterizations used were therefore discussed and further analyses were proposed using different suites of data. Finally, an assessment of the global carbon sink was calculated from the CO<sub>2</sub>, O<sub>2</sub> and APO observations. The global oceanic and terrestrial carbon sinks were calculated to be 2.7 and 2.3  $\text{Pg C yr}^{-1}$ , respectively for the study period 1999-2012.

## Table of Contents

1	Introduction.....	6
2	Background and aims of the project .....	8
2.1	The global carbon cycle .....	8
2.2	Estimating the terrestrial and oceanic carbon sinks .....	10
2.3	Atmospheric Potential Oxygen .....	12
2.4	The Southern Ocean.....	13
2.5	Aims of this research.....	15
2.5.1	Specific objectives of WP1 .....	15
2.5.2	Specific objectives of WP2 .....	15
3	Data and Methods .....	17
3.1	Work Package 1: .....	17
3.1.1	Atmospheric O <sub>2</sub> and CO <sub>2</sub> observations.....	17
3.1.2	Hpspline curve fitting procedure .....	20
3.1.3	ENSO and SAM Climate Indices .....	20
3.2	Work Package 2: .....	20
3.2.1	Identifying carbon cycle events from O <sub>2</sub> and CO <sub>2</sub> observations for the period 1999-2012.....	20
3.2.2	Conceptual model of air-sea gas exchange.....	22
3.2.3	Air mass back-trajectory analysis.....	23
3.2.4	Satellite Net Primary Productivity Estimates .....	27
3.2.5	Argo Float Profile Mixed Layer Depth Estimates .....	29
3.2.6	Dissolved O <sub>2</sub> depth profiles for the Southern Ocean .....	30
4	Results and Discussion .....	32
4.1	Introduction.....	32
4.2	Atmospheric O <sub>2</sub> , CO <sub>2</sub> and APO Observations 1999-2012.....	32
4.2.1	General Trends .....	32
4.2.2	Seasonal variability .....	35
4.2.3	The inter-annual variability of APO .....	35
4.3	Identifying NPP and ventilation events from atmospheric observations.....	40
4.3.1	Annual variability of identified events .....	40
4.3.2	Monthly and seasonal variability of identified events .....	43
4.4	Characterising NPP and ventilation events .....	45
4.4.1	Magnitude of APO change ( $\Delta$ APO).....	45
4.4.2	O <sub>2</sub> :CO <sub>2</sub> molar exchange ratio. ....	47
4.5	Conceptual model of air-sea gas exchange .....	49
4.5.1	Origin of air masses arriving at Baring Head .....	49
4.5.2	Testing the conceptual model.....	51
4.5.3	Example NPP and ventilation events.....	54

4.5.4	Limitations of the conceptual model.....	57
5	Conclusions.....	58
5.1	Summary of key findings.....	58
5.2	Suggestions for further research.....	59
6	Reference List.....	60
7	Appendices.....	66

## 1 Introduction

The simultaneous measurement of atmospheric oxygen ( $O_2$ ) and carbon dioxide ( $CO_2$ ) has become an important tool for studying the global carbon cycle in recent decades (e.g Keeling and Shertz, 1992; Keeling et al., 1996; Bender and Battle, 1999; Tohjima et al., 2005; Manning and Keeling, 2006). By combining these species to form the atmospheric tracer atmospheric potential oxygen (APO, see Section 2.3), which is conservative with respect to terrestrial biosphere processes (Stephens et al., 1998), one can discern information on oceanic processes that exert a critical control on the carbon budget of the atmosphere, such as marine net primary production (NPP) (Nevison et al., 2012) and ventilation of upwelling water masses (Hamme and Keeling, 2008). The Earth's oceans currently provide an important carbon 'sink' to atmospheric  $CO_2$  released as a result of human activities and, as such, this sink has been increasing in response to the atmospheric growth rate of  $CO_2$  over recent decades (Le Quéré et al., 2009). There is much scientific debate however, as to whether the efficiency of the ocean carbon sink is now beginning to decrease as our climate system changes (Le Quéré et al., 2007; Watson et al., 2009). The magnitude of the Southern Ocean carbon sink in particular has caused much controversy (e.g Le Quéré et al., 2007, 2008; Zickfield et al., 2008; Law et al., 2008; Lovenduski et al., 2008) due in part to the difficulty in making observations in this isolated region. Baring Head (BHD), New Zealand ( $41^{\circ}25'$  S,  $174^{\circ}52'$  E) provides an ideal location to assess Southern Ocean carbon cycle variability due to the persistence of southerly air masses arriving at the site (Fig 1.1) (Stephens et al., 2013). Continuous atmospheric  $CO_2$  measurements were established here in 1972 (Lowe et al., 1979) whereas continuous atmospheric  $O_2$  measurements were established in 1999 (Manning, 2001).

Although the  $CO_2$  observations from BHD have been recently published by Brailsford et al., (2012) and Stephens et al., (2013), the  $O_2$ , and hence APO observations have not been analysed or presented in peer-reviewed literature. This project will therefore investigate the variability of atmospheric  $O_2$  and  $CO_2$  observations for the period 1999-2012 from BHD and use them to make important deductions on the regional and temporal variability of Southern Ocean carbon cycle processes. As such, this will be the first study to attempt this using the BHD data. To achieve this, I will use a range of data products and data analysis software packages that can be used as tools to study carbon cycle processes and are freely available on the internet. For example, studies of marine NPP in the last 15 years have made use of remotely sensed data derived from satellites (e.g. Balkanski et al., 1999; Yamagishi et al., 2008; Nevison et al., 2012). Whilst oceanic data such as depth profiles of temperature and salinity, derived from the Argo float profile fleet, have become essential for characterising the vertical structure of the world's oceans (Hosoda et al., 2010) and have therefore aided investigations of the global meridional overturning circulation - the mechanism by which heat and biogeochemical species, such as  $CO_2$ , are distributed across the world's oceans (Wunsch and Heimbach, 2006; Talley, 2013). Furthermore, the use of air-mass back-trajectory models, such as the

Hysplit\_4 model of Draxler and Hess (1998), allows one to determine the origin of air masses arriving at any location in the world. Therefore, this model can be used to determine the history of air masses arriving at BHD and hence ascertain whether the atmospheric O<sub>2</sub> and CO<sub>2</sub> observations are recording gas exchange between the ocean and atmosphere. The motivation of this project is to therefore reconcile these freely available datasets and analysis tools with the atmospheric observations made at BHD to determine what can be learnt about the Southern Ocean carbon cycle.

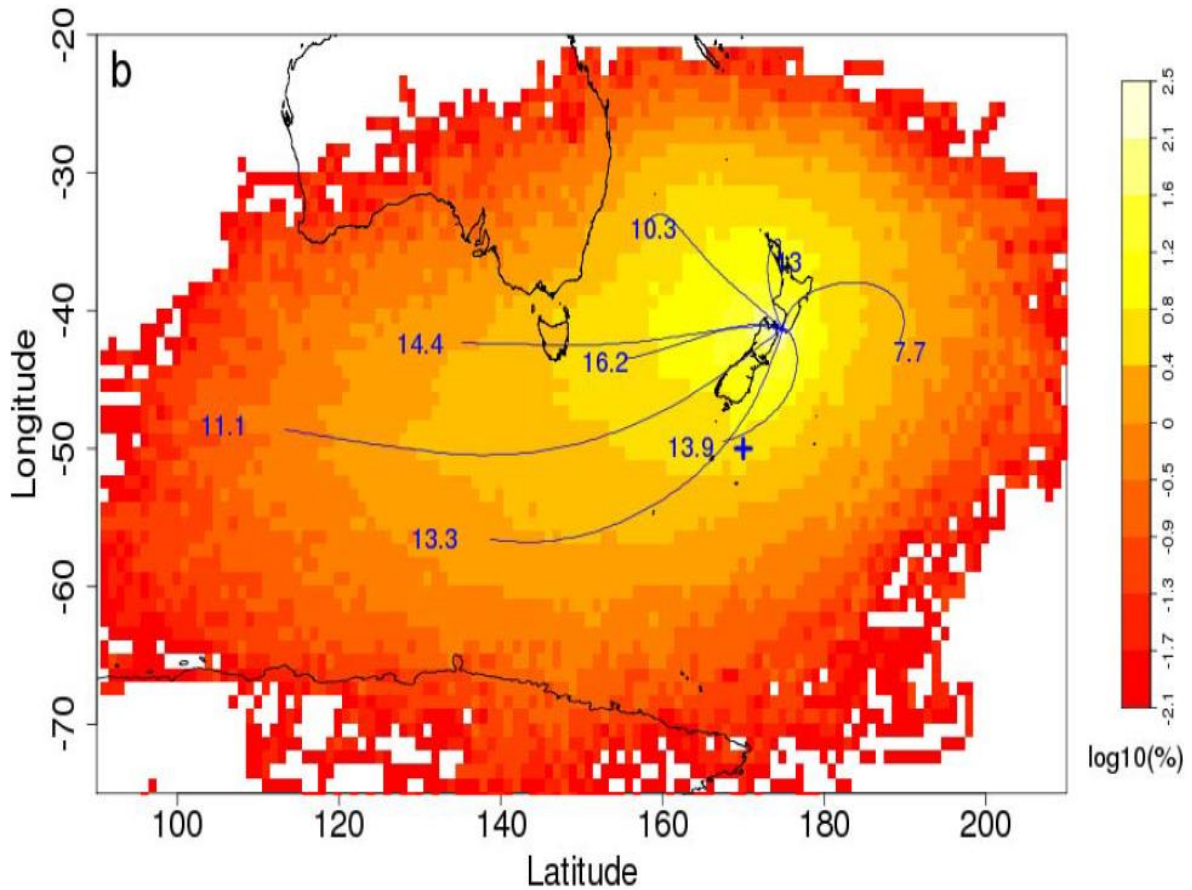


**Figure 1.1** Map showing clustered results of 20 years of twice daily 4-day back-trajectory calculations from Baring Head. Colour shading indicates a logarithm of the percentage of trajectories crossing a given latitude/longitude square. The scale bar on the right spans the range -2.1 to 2.5 log<sub>10</sub>(%). The plus sign refers to an analysis done in the original research paper that this plot appeared in (Stephens et al., 2013). For the purpose of this paper it can be ignored. The plot clearly shows the persistence of south-westerly air masses arriving at Baring Head.

## 2 Background and aims of the project

### 2.1 The global carbon cycle

The global carbon cycle consists of four major reservoirs: the atmosphere, the oceans, the terrestrial biosphere and the geosphere (Fig 2.1). Carbon exchanges between these reservoirs on timescales that range from between a few hours (e.g. photosynthesis) to many millions of years (e.g. sedimentation of organic matter on the seabed and its subsequent subduction into the Earth's interior) (Berner, 1998). The carbon cycle is intimately linked to global climate due to the properties of the major atmospheric carbon species: primarily CO<sub>2</sub> and to a lesser, but still significant extent, methane (CH<sub>4</sub>) and carbon monoxide (CO). Svante Arrhenius (1895) was the first to consider the radiative effects of CO<sub>2</sub>, that is, its ability to absorb and subsequently re-emit long-wave, infrared radiation, upon the surface temperature of the Earth. This is commonly referred to as the 'greenhouse' effect and is also caused and amplified by other atmospheric constituents; primarily water vapour, CH<sub>4</sub> and nitrous oxide (N<sub>2</sub>O). The greenhouse effect is critical to the habitability of Earth and results in an average surface temperature of ~15°C; without it the surface temperature would be closer to -18°C (Hansen, 1984). The average surface temperature of the Earth throughout geological history however, has been far from constant (e.g. Zachos et al., 2001). Even miniscule variations in the relative abundance of the major greenhouse gases have the ability to significantly alter the temperature of the planet.

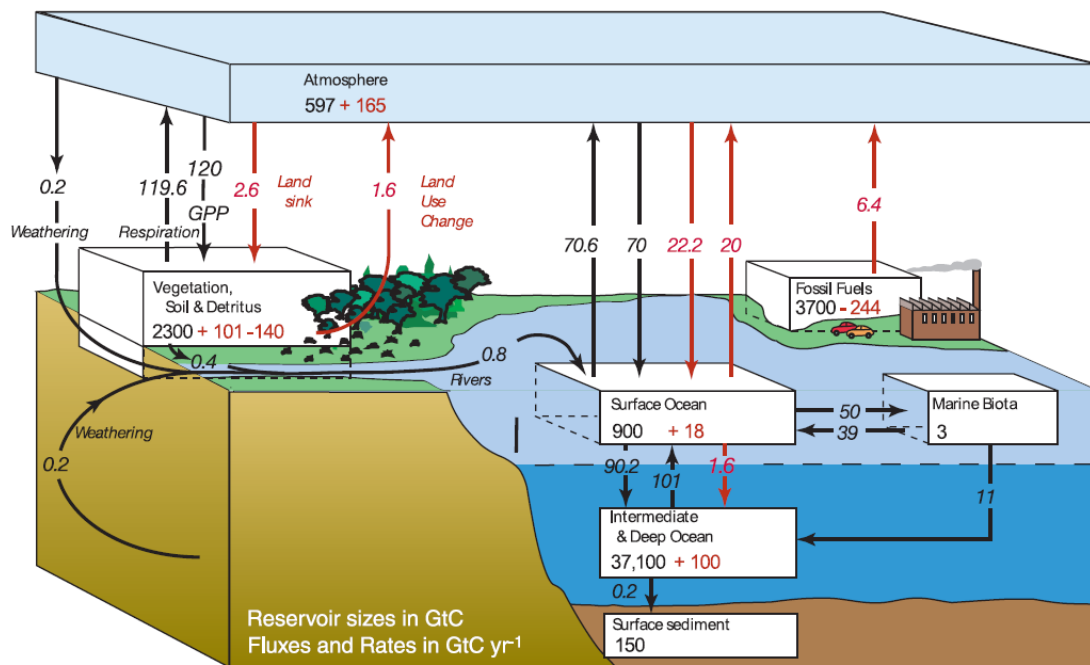


Figure 2.1. The global carbon cycle and the relative fluxes of carbon (C) between the reservoirs in Giga (10<sup>9</sup>) tonnes of C (equivalent to Peta (10<sup>15</sup>) grams of C) per year. Reservoir size (numbers inside the boxes) is given in GtC. Black arrows and numbers indicate natural fluxes whilst red arrows and numbers indicate anthropogenic fluxes. From IPCC AR4 (2007).

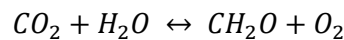
Analysis of ice core records from the Vostok ice core, Antarctica, have shown the co-variation of CO<sub>2</sub> and temperature through the glacial-interglacial cycles of the Quaternary period (~2.6 – 0.01 Million years ago (Ma)) (Petit et al., 1999; Siegenthaler et al., 2005). Both temperature and CO<sub>2</sub> concentrations fluctuated with a period between approximately 20-100 kyrs as a result of natural, orbital induced changes to the amount of solar radiation reaching the Earth's surface. Although the initial change in temperature was forced by changes in solar radiation reaching the Earth's surface, the magnitude of the total temperature change between these cycles cannot be accounted for unless they are amplified by changes to the relative abundance of greenhouse gases, controlled by complex carbon-climate feedback mechanisms (for a review see Sigman and Boyle, 2000). CO<sub>2</sub> concentrations were low during the glacial periods (180 ppm) and high during the inter-glacials (280 ppm) (Siegenthaler et al., 2005). The Southern Ocean in particular is believed to have exerted a critical control over these glacial-interglacial atmospheric CO<sub>2</sub> changes (Watson and Garabato, 2006).

Following the end of the last glacial (~11ky), CO<sub>2</sub> concentrations remained relatively stable at 280 ppm until the beginning of the industrial era (~1750AD), at which point they began to rise. CO<sub>2</sub> concentrations are now ~400 ppm (May 2013, <https://scripps.ucsd.edu/news/7992>) primarily due to the burning of fossil fuels, cement production and land use change, such as deforestation, biomass burning, crop production and conversion of grassland to cropland (IPCC, 2007). These exceptionally high (relative to the last few million years) CO<sub>2</sub> concentrations have been unequivocally warming our climate over recent decades (Hansen et al., 1997; Solomon et al., 2007), and will continue to do so unless the above anthropogenic activities are curtailed (IPCC, 2007).

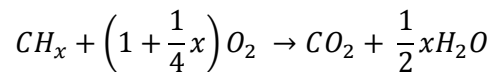
Despite continuous warnings from the scientific community on the potential short-term, centennial scale consequences of rising CO<sub>2</sub> emissions to the Earth's climate system (IPCC, 2001, 2007), we appear to be stubbornly sticking to the "business as usual" scenario (CO<sub>2</sub> emissions in 2010 = 9.1 Pg C yr<sup>-1</sup> (Peters et al., 2012)) first set out by the Inter-governmental Panel on Climate Change (IPCC) in 1992 (predicted emission rate of 8.7 Pg C yr<sup>-1</sup> for 2010 based on IS92a scenario (Pepper et al., 1992)). The expected atmospheric increase in CO<sub>2</sub> concentrations however, is less than that predicted from that of fossil fuel burning alone (approximately 57% of the expected trend (Gloor et al., 2010)). This is because CO<sub>2</sub> is removed from the atmosphere by the Earth's terrestrial and oceanic carbon sinks (1.2 ± 0.8 Pg C yr<sup>-1</sup> and 1.9 ± 0.6 Pg C yr<sup>-1</sup>, respectively for the 10 year period 1990-2000) (Sabine et al., 2004; Manning and Keeling., 2006). If we are to reliably predict future climatic changes, mitigate and adapt to them, it is essential that we characterise and monitor the efficiency of both the terrestrial and oceanic carbon sinks' ability to withdraw anthropogenic CO<sub>2</sub> from the atmosphere, which may change in the future (Le Quéré et al., 2007).

## 2.2 Estimating the terrestrial and oceanic carbon sinks

Different techniques have been employed to estimate the uptake of anthropogenic CO<sub>2</sub> by both the terrestrial and oceanic carbon sinks. These include the use of surface ocean pCO<sub>2</sub> data (Takahashi et al., 2006), <sup>13</sup>CO<sub>2</sub>/<sup>12</sup>CO<sub>2</sub> data (Gruber et al., 1999) and the application of inverse atmospheric transport models (Le Quéré et al., 2007). One of the more unique approaches to this problem involves the simultaneous measurement of atmospheric O<sub>2</sub> and CO<sub>2</sub> concentrations as first outlined by Machta (1980). Ralph Keeling advanced these techniques in his first paper on the subject (Keeling, 1988) and in those that followed (e.g. Keeling and Shertz, 1992; Keeling et al., 1993; Keeling et al., 1996). R. Keeling demonstrated the insight atmospheric O<sub>2</sub> measurements could give to global carbon cycle studies by highlighting the fact that the sources and sinks of CO<sub>2</sub> and O<sub>2</sub> to and from the atmosphere, are stoichiometrically linked through the oxidation and reduction of organic matter, whereby a sink for O<sub>2</sub> will have a corresponding CO<sub>2</sub> source and vice versa: firstly through the processes of photosynthesis and respiration:

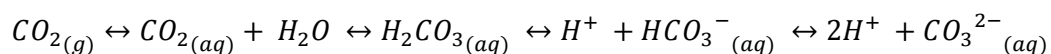


Where CH<sub>2</sub>O is the approximate composition of organic matter, and secondly through combustion of fossil organic matter (i.e. coal, oil and gas) (Keeling, 1988):



The ratio of the exchange (moles of O<sub>2</sub> consumed to moles of CO<sub>2</sub> released (O<sub>2</sub>:CO<sub>2</sub>)) depends on the oxidation state of the organic matter (Keeling, 1988). For photosynthesis and respiration this ratio has value of 1.10 ± 0.05 (Servinghaus, 1995) whereas for fossil fuel combustion the globally weighted average is 1.39 (Manning and Keeling, 2006) but varies depending on the fossil fuel used (1.95 for gaseous fuels to 1.17 for solid fuels).

Both O<sub>2</sub> and CO<sub>2</sub> exchange between the atmosphere and ocean too, however the stoichiometric coupling breaks down due to differences in their seawater chemistry and in the timescale of air-sea exchange (see Keeling, 1988, Keeling et al 1993 and Bender and Battle, 1999): when CO<sub>2</sub> dissolves in seawater it rapidly reacts with water to form carbonic acid which then dissociates into bicarbonate and carbonate ions according to the following equation:



This reaction, specifically the production of H<sup>+</sup> ions, is the reason for ocean acidification as a result of increasing atmospheric CO<sub>2</sub> concentrations (Doney et al., 2008). Importantly, this sink for CO<sub>2</sub> does not have a corresponding source of O<sub>2</sub>, and the lack of a similar seawater chemistry for O<sub>2</sub> results in a much smaller effective solubility in seawater than for CO<sub>2</sub> (Broecker and Peng, 1982; Keeling, 1988). Although CO<sub>2</sub> and O<sub>2</sub> are stoichiometrically linked in marine biological production (O<sub>2</sub>:CO<sub>2</sub> = 1.4, (Anderson, 1995)), the resulting change in seawater CO<sub>2</sub> is heavily suppressed due to the carbonate

chemistry reaction. Moreover, the decoupling between these two species in air-sea exchange is further exacerbated by differences in their equilibration timescales. This is approximately 1 year for CO<sub>2</sub>, whereas O<sub>2</sub> equilibrates much faster on timescales of a few weeks (Broecker and Peng, 1982).

On longer timescales, O<sub>2</sub> measurements can be used to estimate the relative magnitude of both the terrestrial biosphere sink and oceanic sink (Keeling, 1988; Keeling and Shertz, 1992; Keeling et al 1996). Although the increase in atmospheric CO<sub>2</sub> mixing ratios due to fossil fuel burning drives a flux of CO<sub>2</sub> into the ocean, as described above, the corresponding decrease in O<sub>2</sub> mixing ratios does not drive a flux of O<sub>2</sub> out of the oceans because the oceans' capacity for O<sub>2</sub> is too small, since 99% of the total amount of O<sub>2</sub> in the atmosphere-ocean system resides in the atmosphere (Keeling, 1988; Bender and Battle, 1999).

Hence, by removing the fossil fuel component from the long term atmospheric O<sub>2</sub> signal, one knows that the residual signal must be due to terrestrial biosphere exchange. One can then estimate the corresponding terrestrial CO<sub>2</sub> sink from the oxidative ratio of 1.1 for the terrestrial biosphere (Severinghaus, 1995) and hence, by deduction, estimate the oceanic carbon sink (Keeling, 1988; Keeling and Shertz, 1992; Keeling et al., 1993, 1996; Bender et al., 1998). Keeling and Shertz (1992) were the first to attempt this analysis and estimated that the oceans and terrestrial biosphere each removed approximately 30% of fossil fuel CO<sub>2</sub>. Table 2.1 shows more recent studies based on this method of the global land and oceanic carbon sinks.

**Table 2.1 Recent estimates of the land and ocean carbon sink.**

Study	Land Carbon Sink (Pg C yr <sup>-1</sup> )	Ocean Carbon Sink (Pg C yr <sup>-1</sup> )	Time period	Stations
Bender et al., (2005)	1.0 ± 0.6	1.7 ± 0.5	1994-2002	Barrow, American Samoa, Cape Grim.
Manning and Keeling, (2006)	0.5 ± 0.7	2.2 ± 0.6	1993-2003	Alert, La Jolla, Cape Grim
Tohjima et al., (2008)	1.0 ± 0.9	2.1 ± 0.7	1999-2005	Hateruma Island, Cape Ochi-Ishi
Ishidoya et al., (2012)	0.8 ± 0.9	2.9 ± 0.7	2001-2009	Ny-Ålesund, Svalbard, Syowa

On seasonal timescales, atmospheric observations of CO<sub>2</sub> concentrations are characterised by a seasonal variation driven by the terrestrial biosphere. Whereas atmospheric O<sub>2</sub> observations have a seasonal variation driven by both the terrestrial biosphere *and* oceanic exchange influenced by spring/summer marine biological production, winter ventilation of deep O<sub>2</sub>-deficient, carbon-rich subsurface waters as the seasonal thermocline breaks down and a seasonal thermal component (Bender and Battle, 1999). Therefore, on seasonal timescales, one can remove the seasonal component of the terrestrial biosphere from the O<sub>2</sub> observations by comparison with the CO<sub>2</sub> observations, leaving a residual O<sub>2</sub> component that is driven solely by oceanic processes (Keeling 1988; Keeling and Shertz, 1992; Bender and Battle, 1999). Using three years of O<sub>2</sub> flask sample data from Alert, Canada, La Jolla, U.S.A., and Cape Grim, Australia from 1989 to 1992, Keeling and Shertz (1992)

discovered that the residual seasonal O<sub>2</sub> signal (after removing the terrestrial biosphere influence) was largely driven by marine biological production (85%) in the summer with a smaller but still significant thermal outgassing signal (15%), and driven by the seasonal break down of the thermocline in winter months, leading to ventilation of O<sub>2</sub> deficient waters. This work was later corroborated by Bender et al., (1996) on O<sub>2</sub> flask sample data from Cape Grim, Tasmania and Baring Head, New Zealand.

### **2.3 Atmospheric Potential Oxygen**

Stephens et al., (1998) derived the atmospheric tracer Atmospheric Potential Oxygen ( $APO = \Delta O_2 + 1.1\Delta CO_2$ ). The factor 1.1 accounts for the O<sub>2</sub>:CO<sub>2</sub> stoichiometric ratio for land biotic photosynthesis and respiration (Severinghaus, 1995) and hence APO, by definition, is conservative to terrestrial biosphere influences (Stephens et al., 1998). Variability in APO is therefore influenced by fossil fuel combustion, which drives a decrease in APO values since the oxidative ratio for combustion is >1.1 and oceanic processes, which drive the seasonal variability in APO (Stephens et al., 1998). In their analysis, Stephens et al., (1998) calculated the inter-hemispheric gradient in APO from seven stations recording atmospheric O<sub>2</sub> and CO<sub>2</sub> observations and compared the results to an ocean biogeochemical models of air-sea fluxes coupled to an atmospheric transport model. They discovered the models significantly underestimated the inter-hemispheric gradient of APO and proposed that the models must be underestimating the net southward oceanic transport of both O<sub>2</sub> and CO<sub>2</sub>. Conversely, Gruber et al., (2001) performed a similar study but used an inverse modelling technique that is independent of air-sea gas exchange parameterizations. Through their analysis, Gruber et al., (2001) discovered the inter-hemispheric transport of O<sub>2</sub> can be described by the existence of two closed asymmetric circulation cells of O<sub>2</sub> transport from the mid-to-high latitudes towards the tropics, where O<sub>2</sub> is out gassed from the ocean at the equator and transported back to the poles through the atmosphere. The northern hemisphere cell is stronger than that in the southern hemisphere, resulting in increased O<sub>2</sub> uptake in northern temperate regions (Gruber et al., 2001). This asymmetry in the two circulation cells, combined with the asymmetry in fossil fuel emissions (greater in the northern hemisphere) can account for the inter-hemispheric APO gradient more accurately than the analysis proposed by Stephens et al., (1998) (Gruber et al 2001).

The modelling studies of Stephens et al. (1998) and Gruber et al. (2001) imply a strong equatorial out gassing of O<sub>2</sub> that produces an equatorial “bulge” in APO that could not be confirmed due to a lack of observations in this region. Tohjima et al., (2005) subsequently confirmed this prediction using shipboard flask measurements of O<sub>2</sub> and CO<sub>2</sub> collected across the western Pacific Ocean between Japan and the United States and Japan and Australia. For a review of the current state of global APO distributions and variability see Battle et al., (2006), who presented the first global observations of

APO for the period 1996-2003 with a comprehensive review of how they compare to current atmosphere-ocean modelling approaches of global APO distributions.

Although these initial studies have been useful in determining global and inter-hemispheric trends in APO, very little work has been done on constraining its regional, seasonal and inter-annual variability, with the exception of the studies that I will discuss below. Investigations at these spatial and temporal scales are critical if we want to assess the finer details of the oceanic carbon sink, particularly as some studies are now pointing toward a weakening of this sink (Le Quéré et al., 2007; Watson et al., 2009) and hence there is a clear need for more *in situ* atmospheric observations.

Yamagishi et al., (2008) present the only study to date of temporally short (daily) variations of APO from in-situ measurements of O<sub>2</sub> and CO<sub>2</sub> at Cape Ochi-Ishi, Japan. Their analyses focused on explaining peaks in APO values recorded between April and July, 2005 by computing air-mass back trajectories to determine the path of the air masses arriving at Cape Ochi-Ishi and by comparing these paths to monthly-averaged marine NPP estimates derived from satellite observations of the Okhotsk Sea and the western North Pacific (Yamagishi et al., 2008). Their results indicated that APO values were high (low) when air-masses had passed over productive (unproductive) regions of the ocean, corroborating the fact the APO variations are largely driven by marine biosphere processes (Yamagishi et al., 2008). The analysis presented in my project will therefore be similar to that of Yamagishi et al. (2008), except I will also identify ventilation events in addition to NPP events and analyse a much larger APO dataset from BHD for the period 1999-2012.

## **2.4 The Southern Ocean**

The Southern Ocean is a critical component of the global carbon cycle, currently accounting for ~40% of the global ocean uptake of anthropogenic CO<sub>2</sub> (~0.7 Pg C yr<sup>-1</sup>) (Sabine et al., 2004; Mikaloff Fletcher et al., 2007). When attempting to understand the Southern Ocean carbon cycle however, one needs to consider oceanic transport within the region. Strong westerly winds that encircle the Antarctic continent exert a significant stress upon the surface of the ocean centred along the axis of the eastward flowing Antarctic Circumpolar Current (ACC) (Rintoul et al., 2011). To the south of the ACC, Ekman transport creates a divergence that allows the upwelling of deep waters rich in dissolved inorganic carbon (Rintoul et al., 2011). Degassing of these waters therefore constitutes a significant source of 'natural' CO<sub>2</sub> to the atmosphere (Mikaloff Fletcher et al., 2007). North of the ACC, Ekman transport is convergent and surface waters are subducted into the ocean interior as Sub-Antarctic Mode Water and Antarctic Intermediate Water (Rintoul et al., 2011). It is the formation of these water masses that constitute the largest contribution to the uptake and storage of anthropogenic CO<sub>2</sub> within the Southern Ocean ( $0.42 \pm 0.2$  Pg C yr<sup>-1</sup>) (Sabine et al., 2004, Salle et al., 2012).

Monitoring the variability of these processes is an inherently difficult task given the scarcity of observations in this isolated region and consequently, is the source of much recent scientific debate (e.g. Le Quéré et al., 2007, 2008; Law et al., 2008; Zickfield et al., 2008; Roy et al., 2003; Metzl et al., 2006). Le Quéré et al., (2007), using an inverse method combined with observed atmospheric CO<sub>2</sub> concentrations, concluded that the overall Southern Ocean sink for CO<sub>2</sub> had declined by 0.08 Pg C yr<sup>-1</sup> decade<sup>-1</sup> for the period 1981-2004, relative to the trend that would otherwise be expected from the increased atmospheric CO<sub>2</sub> burden. The model of Le Quéré et al., (2007) suggested this was due to an increase in the degassing of natural carbon south of the ACC as a result of strengthening winds over the Southern Ocean that are thought to be the result of human activities (Le Quéré et al., 2007; Thompson and Solomon, 2002; Shindell and Schmidt, 2004). However, both Law et al., (2008) and Zickfield et al., (2008) contested these findings. The former suggested that the results were very much dependent on both the choice of ocean model and the network of observations employed (Law et al., 2008). Hence, if there is such a bias due to the choice of sites used then more atmospheric observation sites, such as those at BHD, will surely reduce this bias. The latter argued that the altered Southern Ocean winds, coincident with rising atmospheric CO<sub>2</sub> levels will likely increase the Southern Ocean sink in the 21<sup>st</sup> century (Zickfield et al., 2008). Lovenduski et al., (2008), using output from hindcast simulations of an ocean circulation model with embedded biogeochemistry, found a similar decrease in the efficiency of the Southern Ocean carbon sink to Le Quéré et al., (2007) and also concluded strengthening of the westerly winds were a likely cause.

The increase in the westerly wind strength has been attributed to a trend towards a more persistent positive phase in the Southern Annular Mode (SAM) (Thompson and Solomon, 2002), which is characterised by a trend toward falling atmospheric pressure of the pole and a corresponding rise in pressure over the mid-latitudes. Furthermore, atmospheric inverse models (Butler et al., 2007) and ocean biogeochemistry models (Lenton and Matear, 2007; Lovenduski et al., 2007) suggest anomalous Southern Ocean CO<sub>2</sub> outgassing of ~0.1 Pg C yr<sup>-1</sup> per standard deviation of the SAM index. One aspect of this project will therefore investigate whether an increase in the frequency of ventilation events, identified in the atmospheric O<sub>2</sub> and CO<sub>2</sub> data, is observed during periods of a particularly strong positive phase of the SAM. I will also investigate whether a similar correlation can be observed with El-Nino-Southern Oscillation (ENSO) given that previous studies (Le Quéré et al., 2003; Verdy et al., 2007) have shown that this also influences the Southern Ocean westerlies and hence the upwelling and ventilation of carbon rich deep waters.

According to Takahashi et al., (2012) the regions of NPP within the Southern Ocean are centred along the latitude of 30°S. On the other hand, regions of upwelling and hence ventilation of CO<sub>2</sub> rich, O<sub>2</sub>-deficient waters are located further south, along the latitude of 50°S (Takahashi et al., 2012). This project will therefore determine whether air masses arriving at BHD are sampling the regions defined

by Takahashi et al., (2012) by performing an air mass back-trajectory analysis. If so, then I will attempt to answer the following questions: What are the general characteristics of the APO observations when air is being sampled from these particular regions? Do the APO observations vary on annual and seasonal timescales when air is being sampled from these regions? Can the APO observations be reconciled with satellite NPP estimates and proxies for the ventilation of CO<sub>2</sub> rich, O<sub>2</sub> deficient water masses in the regions identified in the air mass history? Finally, although the primary goal of investigations assessing the state of the global carbon cycle is to determine the year to year variations in atmospheric CO<sub>2</sub> sinks, it is not the main objective of this project. Instead, I seek to determine whether current datasets and analysis tools used in investigations of the carbon cycle can be reconciled and further assess what can be achieved through study at the spatial and temporal resolution discussed.

## **2.5 Aims of this research**

The aim of this project is to investigate the spatial and temporal variability of carbon cycle processes in the vicinity of the Southern Ocean using observations of atmospheric O<sub>2</sub> and CO<sub>2</sub> from Baring Head, New Zealand. This will be done by achieving the following work packages:

**Work Package 1 (WP1):** Investigate the overall characteristics of the atmospheric O<sub>2</sub> and CO<sub>2</sub> observations recorded at BHD for the period 1999-2012 and determine the inter-annual variability in APO, assessing whether a correlation can be found with the dominant modes of climate variability within the Southern Ocean.

### *2.5.1 Specific objectives of WP1*

1. Perform an Hpspline analysis (see below) to break down the CO<sub>2</sub>, O<sub>2</sub> and APO signals into the following components: a). Overall trend; b). Seasonal; c). Deseasonalised-detrended and d). The residual.
2. Determine whether a correlation exists between said components and the ENSO or SAM indices.

Information discerned in WP1 will then be used to aid in the interpretation of Work Package 2.

**Work Package 2 (WP2):** Characterisation of the variability and origin of carbon-cycle process on weekly timescales.

### *2.5.2 Specific objectives of WP2*

1. Identify the signal of a). Ocean primary productivity; and b). Ocean ventilation within the continuous BHD APO dataset for the period 1999-2012.

2. Assess whether a common atmospheric O<sub>2</sub>:CO<sub>2</sub> ratio can be observed from the recorded ocean primary productivity and ventilation events.
3. Determine the origin of said processes through air-mass footprint analysis and through the investigation of satellite ocean productivity data, Argo float profile data and depth profiles of dissolved O<sub>2</sub> concentrations in the Southern Ocean.
4. Develop a simple conceptual model of air-sea gas exchange to determine whether the independent data-sets in (3.) can be reconciled with the atmospheric observations at BHD.

### 3 Data and Methods

#### 3.1 Work Package 1:

*Investigate the overall characteristics of the atmospheric O<sub>2</sub> and CO<sub>2</sub> observations recorded at BHD for the period 1999-2012 and determine the inter-annual variability in APO, assessing whether a correlation can be found with the dominant modes of climate variability within the Southern Ocean*

##### 3.1.1 Atmospheric O<sub>2</sub> and CO<sub>2</sub> observations

###### 3.1.1.1 The Baring Head Atmospheric Observatory

Atmospheric measurements were collected from the atmospheric observation site located at Baring Head, New Zealand (41.41°S, 174.87°E), ~10 km southeast of the city of Wellington (Fig 3.1) for the period 1999-2012. The O<sub>2</sub> and CO<sub>2</sub> measurement system is housed in a small concrete building close to the edge of a south facing coastal cliff, approximately 240 m from the ocean at a height of 85 m above sea level (Stephens et al., 2013). Air is sampled from a pair of air intakes at the top of a 10 m tall tower adjacent to the building. The air is subsequently dried and held at a constant temperature and pressure before being fed in to the respective O<sub>2</sub> and CO<sub>2</sub> analysers. CO<sub>2</sub> was measured using a non-dispersive infrared (NDIR) analyser, established at the site by Charles Keeling's group from the Scripps Institution of Oceanography (SIO), California, in collaboration with the National Institute for Water and Atmospheric Research (NIWA), New Zealand in 1972 (Lowe et al., 1979). O<sub>2</sub> was measured using a paramagnetic O<sub>2</sub> analyser established at the site by Andrew Manning, then at SIO, in 1999 (Manning, 1999).

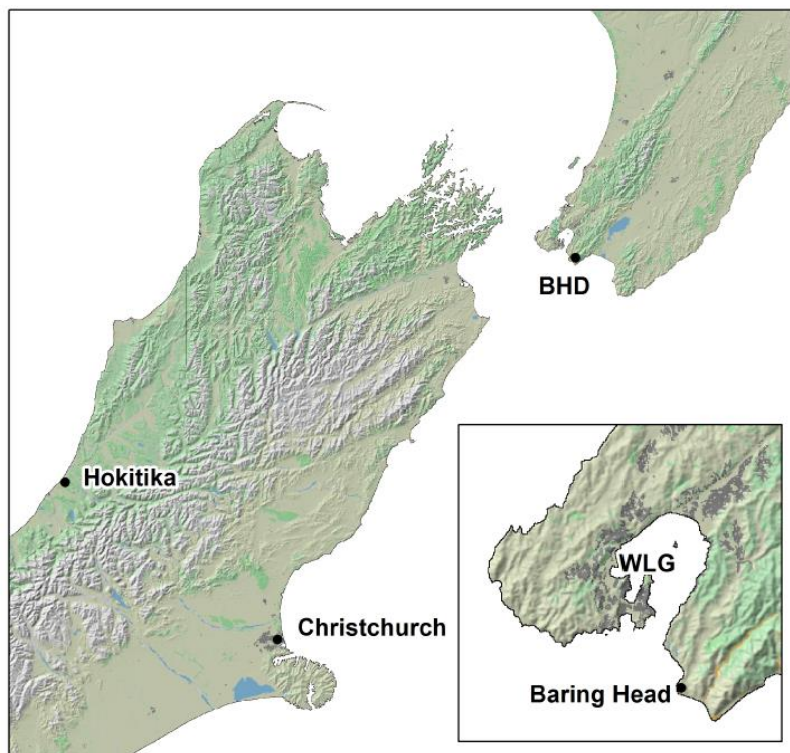


Figure 3.1. Location of Baring Head (BHD) at the southern tip of the North Island, New Zealand.

The level of relative precision required for atmospheric O<sub>2</sub> measurements is very high since one needs to detect changes in O<sub>2</sub> partial pressure on the order of 1 in 10<sup>6</sup>, hence, changes in the partial pressure of other gases in the air will affect the O<sub>2</sub> measurement (Keeling and Shertz, 1992). O<sub>2</sub> concentrations are therefore reported on a relative scale calculated as the change in the ratio of O<sub>2</sub> to nitrogen (N<sub>2</sub>) relative to a standard O<sub>2</sub> to N<sub>2</sub> ratio. This value is subsequently multiplied by 10<sup>6</sup> and expressed in “per meg” units so as to accommodate the miniscule variations in O<sub>2</sub> concentrations:

$$\delta(O_2/N_2) = \frac{(O_2/N_2)_{\text{sam}} - (O_2/N_2)_{\text{ref}}}{(O_2/N_2)_{\text{ref}}} \times 10^6$$

Measurements are made every 5 minutes. The resulting data are then run through an Interactive Data Language (IDL) routine which removes any erroneous data points, such as when there were known problems with the analysers or calibration procedures, as noted by the site technicians. The IDL routine also produces an array of plots showing CO<sub>2</sub>, O<sub>2</sub> and APO (O<sub>2</sub>+1.1CO<sub>2</sub>) concentrations at different temporal scales: yearly, monthly, weekly and daily with additional plots showing the meteorological conditions recorded at the site at the time of sampling (Fig 3.2).

The IDL routine for filtering and plotting data was written by my supervisor, Andrew Manning, and other members of his group. My contribution was to produce new plots of O<sub>2</sub> vs CO<sub>2</sub> concentrations, colour-coded to represent the time of measurement, whilst attempting to develop a methodology for the identification and characterisation of ‘events’ (top right hand plot in the images a-e in Fig 3.2). The aim of doing this was to eventually produce a least-squares linear best fit to the data to ascertain the ratio of the O<sub>2</sub> to CO<sub>2</sub> concentrations and so determine whether a common exchange ratio could be found in oceanic carbon cycle events like those found for fossil fuel burning (Keeling, 1993) and terrestrial biosphere exchange (Severinghaus, 1995). A least-squares linear best fit is calculated based on the error in both the x and y direction, whereas a typical line of best fit calculation, such as those used in Excel, only base the fit on the error in the y direction and hence would not result in the correct O<sub>2</sub>:CO<sub>2</sub> exchange ratio. Unfortunately, developing this particular bit of IDL code proved both difficult and time-consuming and therefore had to be omitted from this thesis. This work is an ongoing process however, and will be developed for planned follow up work to that presented in my thesis.

The second plot I developed (bottom right hand plot in the images a-e in Fig 3.2) is a histogram of the molar O<sub>2</sub>:CO<sub>2</sub> ratio and was produced for the same reasons as above. Unfortunately, as the data analysis progressed, these plots were not relied upon to determine the molar exchange ratio of oceanic carbon cycle events. Instead I opted for a simpler method where the ratio was determined based on the difference between the start and end point concentrations of O<sub>2</sub> and CO<sub>2</sub> (see Section 3.2.1).

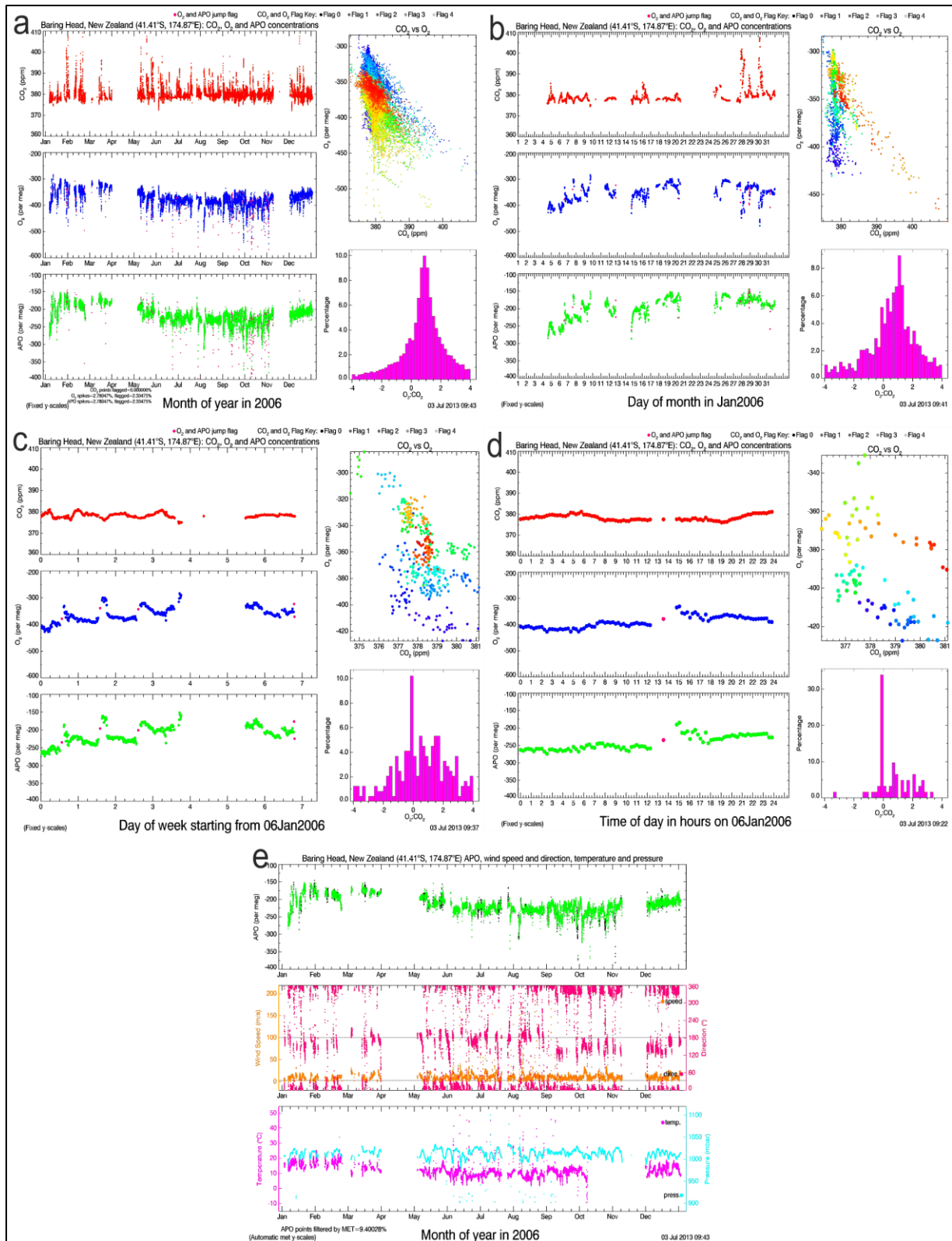


Figure 3.2 . The array of plots used to visualise the BHD CO<sub>2</sub> (red data), O<sub>2</sub> (blue data) and APO (green data) atmospheric observations at different temporal frequencies: (a) = yearly; (b) = monthly; (c) = weekly; (d) = daily. Plot (e) displays the meteorological variables (panels 2 and 3) recorded simultaneously with the atmospheric observations.

### *3.1.2 Hpspline curve fitting procedure*

The Fortran procedure consists of fitting data to a harmonic function and a 3<sup>rd</sup> order polynomial equation plus a cubic spline (Reinsch, 1967). The procedure was provided by Penelope Pickers, a PhD student of my supervisor, Andrew Manning. The O<sub>2</sub>, CO<sub>2</sub> and APO data were run through the procedure using a harmonic function consisting of 4 harmonics. The procedure then generated the de-seasonalised trend component, the de-trended seasonal component and a residual, representing the inter-annual variability, for each of the atmospheric species.

### *3.1.3 ENSO and SAM Climate Indices*

The inter-annual variability in APO was then compared against the Southern Annual Mode (SAM) index, using data provided by David Thompson and Jonathan Woodworth, both of Colorado State University, U.S. (<http://www.atmos.colostate.edu/ao/Data/>). The SAM is characterized by changes in atmospheric mass between 20°S and 90°S, and is defined by the pressure difference recorded at observation stations at these two latitude bands for each month of year for the period 1999-2012 (Marshall, 2003).

The APO data will then be compared to a monthly Multivariate ENSO index (MEI), using data provided by the United States National Oceanic and Atmospheric Administration (NOAA) (<http://www.esrl.noaa.gov/psd/data/climateindices/list/>). The MEI is based on 6 observed variables over the tropical Pacific: sea-level pressure, zonal and meridional components of the surface wind, sea surface temperature, surface air temperature and total cloudiness fraction of the sky (Wolter and Timlin, 1998). The MEI is then calculated as the first Principal Component of all six observed fields combined for each of twelve bi-monthly seasons (Dec/Jan, Jan/Feb, etc). All seasonal values are then standardized with respect to each season and to a 1950-93 reference period (Wolter and Timlin, 1998).

## **3.2 Work Package 2:**

*Characterisation of the variability and origin of carbon-cycle process on weekly timescales.*

### *3.2.1 Identifying carbon cycle events from O<sub>2</sub> and CO<sub>2</sub> observations for the period 1999-2012*

Using the plots generated by the IDL routine (Fig 3.2) I visually identified potential oceanic carbon cycle events for the full record period of 1999-2012. I identify two types of oceanic events, based on the discussion in Section 2 and in Table 3.1, which displays the expected direction of APO change for the respective carbon cycle processes. NPP events are defined as those with a positive excursion in APO and ventilation events are defined as those with a negative excursion in APO. Furthermore, events were selected based on time periods when the winds were from a consistent direction for at least 1 hour. For each event identified, the start and end O<sub>2</sub> and CO<sub>2</sub> concentrations were recorded

(and hence APO) along with the event start and end time (Fig 3.3). As event identification work progressed, it was clear that there was no “model” shape for either a NPP or a ventilation event. As such, the events recorded varied in both duration and in their characteristic shape of the APO excursion. For example Fig 3.3 shows the identification of the start and end point of two events, defined by the red dots: there is a short term excursion in APO over a period of a few hours and a longer-term excursion over a period of a few days. In this case, both excursions are recorded as events. This strategy allows me to identify a range of events that may be influenced by a short term signal but contribute to an overall larger signal that may be more easily reconciled with satellite NPP estimates (See Section 3.2.4) and pO<sub>2</sub> estimates at the depth of the mixed layer (See sections 3.2.5 and 3.2.6).

**Table 3.1** Displaying the expected trends in atmospheric observations with regards to carbon cycle processes addressed in this project.

<u>Carbon Cycle Process</u>		<u>CO<sub>2</sub> trend</u>	<u>O<sub>2</sub> trend</u>	<u>APO trend</u>
<i>Ocean Primary Productivity</i>		↓	↑	↑
<i>Ocean Ventilation</i>		↑	↓	↓
<i>Land Biosphere</i>	<i>Photosynthesis</i>	↓	↑	<i>No Change</i>
	<i>Respiration</i>	↑	↓	<i>No Change</i>

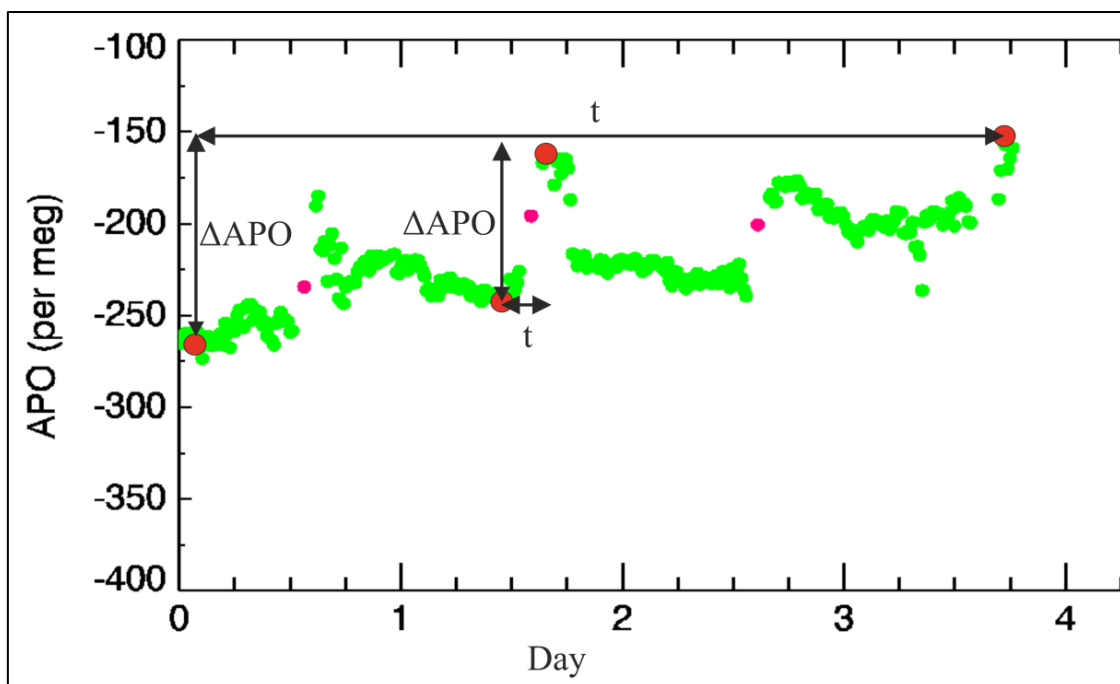


**Figure 3.3** Demonstrating the identification of two potential NPP events in the APO recorded. The magnitude of APO change is displayed ( $\Delta$ APO) is displayed for the duration of the event ( $t$ ).

### 3.2.2 Conceptual model of air-sea gas exchange

For each event identified in the atmospheric O<sub>2</sub> and CO<sub>2</sub> observations, I set out to determine an oceanic region of influence that could explain either the NPP signal or the ventilation signal. To do this, I computed a 4-day air mass back-trajectory, using the Hysplit\_4 model of Draxler and Hess (1998) (see Section 3.2.3). As a first approximation, the region of influence was compared to both satellite NPP estimates from the vertically generalised production model (VGPM) of Behrenfeld and Falkowski (1997) and pO<sub>2</sub> estimates (Garcia et al., 2010) at the MLD (Hosoda et al., 2010) from the Argo float profiling network (see Sections 3.2.4 to 3.2.6) to determine whether the observed APO signal could be explained by either NPP or ventilation of deep waters. The methodology developed for reconciling these various suites of data used in this project is entirely my own. Much of my research time was spent investigating various data-analysis packages, downloaded from the internet, which would help me achieve the aims of my analysis. The research methodology described here is therefore an entirely new approach applied to the investigation of carbon cycle processes inferred from in-situ atmospheric observations.

To aid in the reconciliation of the various datasets used I found it useful to construct a simple conceptual model of air-sea gas exchange over the region of influence defined by the Hysplit\_4 air-mass back-trajectory analysis (Fig 3.4). This model views air-sea gas exchange in an atmospheric ‘puff model’ described by Jacob (1999) and subsequently used in studies of a similar nature to the analysis performed here (Lueker et al., 2003; Thompson et al., 2007; Yamagishi et al., 2008). In this model, I presume the change in APO concentrations recorded over the event are due to O<sub>2</sub> fluxes either into (ventilation signal) or out of (NPP signal) the ocean. As described in Section 2, O<sub>2</sub> exchanges between the ocean and the atmosphere on much quicker timescales compared to CO<sub>2</sub> and, given the timescale of exchange considered here (4 days), it is reasonable to assume that the NPP and ventilation signals recorded in the APO observations are due to O<sub>2</sub> fluxes alone. Equation 1 estimates the flux of O<sub>2</sub> going into/out of the ocean integrated over the region of influence, defined by the back trajectory, over the duration of the event:

$$F = \frac{\rho_a \Delta C h}{t[1 - \exp(-\frac{L}{ut})]} \quad \text{Equation 1}$$

Where F is the sea to air flux of O<sub>2</sub>, ρ<sub>a</sub> = density of air in the planetary boundary layer (PBL) of the troposphere, here assumed to be 40.9 mol m<sup>-3</sup>; ΔC is the change in APO concentration, h is the vertical mixing height; L is the wind fetch, u is the average wind speed over the 4-day period estimated from blended and gridded high resolution global sea surface winds from multiple satellites (Zhang, 2006) (<ftp://eclipse.ncdc.noaa.gov/pub/seawinds/SI>); h is assumed to be the top of the PBL over the ocean in the vicinity of New Zealand, assumed to be 750 m based on the estimates of Denning (2013); L is estimated from the approximate path length of the back-trajectory calculation by

importing an image of the back-trajectory track into Google Earth and then using the path measure tool provided in the software;  $t$  is the time taken for  $C$  to reach  $1/e$  of its total change over the duration of the event, hence  $t$  is defined as:

$$t = \frac{\Delta C/e}{\Delta C/t_e} \quad \text{Equation 2}$$

Where  $t_e$  is the duration of the event.

Using the  $O_2$  flux estimation,  $F$ , I then calculated the  $pO_2$  concentration required to ascertain this flux due to a ventilation event based on the formulation of gas-exchange velocity of Wanninkhof, (1992):

$$F = K \cdot C_w \quad \text{Equation 3}$$

Where  $F$  is the sea to air flux of  $O_2$ ;  $C_w$  is the  $pO_2$  concentration and  $K$  is the transfer velocity defined by:

$$K = 0.39u^2 \left(\frac{Sc}{660}\right)^{-0.5} \quad \text{Equation 4.}$$

Where  $Sc$  represents the Schmidt number for  $O_2$  in seawater at a temperature of  $10^\circ C$  and a salinity of 34.0‰, here taken to be  $0.9216 \times 10^3$  (no units). The derived  $pO_2$  concentration was then compared to the difference between the  $pO_2$  in surface waters and that at the MLD based on  $pO_2$  depth profiles of Garcia et al. (2010) (See Sections 3.2.5 and 3.2.6)

For those events identified as a productivity signal the  $O_2$  flux,  $F$ , was converted to a NPP estimate in  $mg\ C\ m^{-2}\ yr^{-1}$ , based on the molar exchange ratio of  $O_2$  to  $CO_2$  for photosynthesis in marine phytoplankton, here assumed to be  $O_2:CO_2 = 1.4$  (Anderson, 1995), and compared to satellite NPP estimates based on the VGPM model of Behrenfeld and Falkowski (1997).

### 3.2.3 Air mass back-trajectory analysis.

Once all the potential carbon cycle events had been indentified from the atmospheric  $O_2$  and  $CO_2$  observations at Baring Head, I set out to determine the origin of the air mass containing a particular event signal and hence determine a region of influence that could be responsible for the atmospheric observations. To perform such an analysis, I used the HYSPLIT\_4 (HYbrid Single-Particle Lagrangian Integrated Trajectory) model (Version 4) of Draxler and Hess (1998). The Hyplit\_4 model uses previously gridded meteorological data (See Section 3.2.3.2) to determine simple particle trajectories, run either forward or backward, from a particular starting location and time (Draxler and Hess, 1998). Although the model is capable of computing complex dispersion and deposition simulations for the emissions of pollutants (Draxler and Hess, 1998), here I use the model to compute a simple back-trajectory analysis of air particles arriving at the observation station at Baring Head. As

such, I only consider particle advection rather than particle dispersion and deposition within the modelled back trajectories.

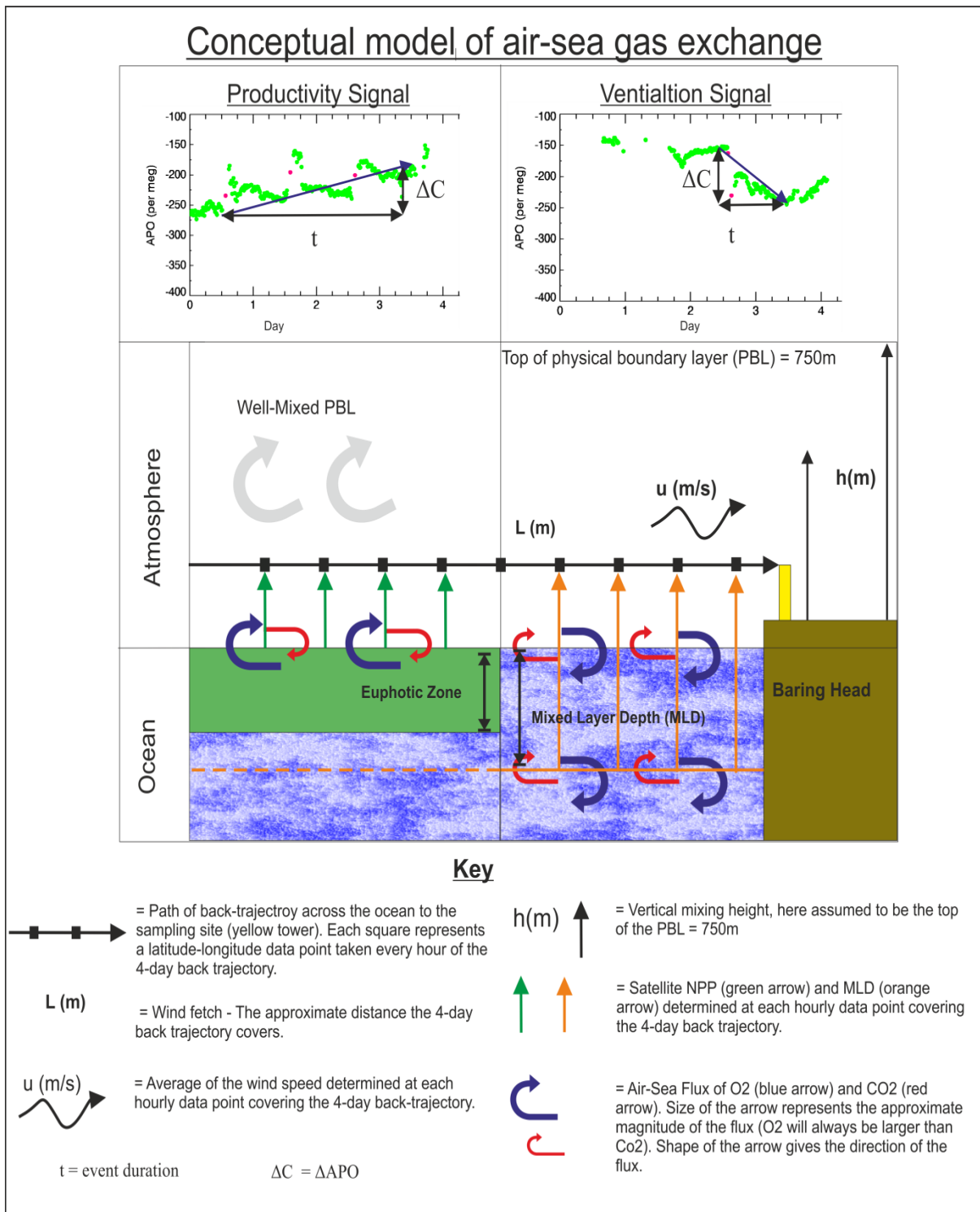


Figure 3.4. Diagram depicting the parameterization of the conceptual model developed in this project. Symbols are defined in the figure and relate to equation 1.

### 3.2.3.1 Advection of air particles

The advection of a particle is computed from the average of the three-dimensional velocity vectors (U,V,W), contained in the meteorological data (see below) for the initial-position P(t) and the first-guess position P'(t+Δt) (Draxler and Hess, 1998). The velocity vectors are therefore linearly interpolated in both space and time, where the first guess position is:

$$P'(t+\Delta t) = P(t) + V(P,t) \Delta t$$

and the final position is:

$$P(t+\Delta t) = P(t) + 0.5 [ V(P,t) + V(P',t+\Delta t) ] \Delta t. \text{ (Draxler and Hess, 1998).}$$

### 3.2.3.2 Meteorological Data

The meteorological data files were obtained from the United States National Oceanic and Atmospheric Administration (NOAA) Air Resources Laboratory (ARL) analysis data archive (<http://ready.arl.noaa.gov/archives.php>) using output from the Global Data Assimilation System (GDAS) (Draxler and Hess, 1998). The GDAS operational system is a meteorological model run by the U.S. National Weather Service's National Centre for Environmental Prediction (NCEP) and contains basic information fields of U and V wind components, temperature and humidity (<http://ready.arl.noaa.gov/gdas1.php>). The model is run four times a day (Midnight, 6AM, Noon and 6PM) and outputs 3, 6 and 9 hour forecasts which are then processed by the NCEP to create global 1 degree latitude-longitude grids of the meteorological data on pressure surfaces. The data are put into weekly files and made available online at the ARL server (<ftp://arlftp.arlhq.noaa.gov/pub/archives/gdas1>) from which I subsequently downloaded the files from. The meteorological data files at this resolution (1-degree, global coverage) are only available from 2006 to present. Hence, only the events identified in the 2006-2012 period had a back-trajectory analysis performed on them.

For each event a 4-day air mass back trajectory was calculated using the ensemble form of the Hysplit\_4 model to determine the air mass history and hence determine the region of influence upon the atmospheric signal. This method automatically starts multiple trajectories from the starting point of the Baring Head atmospheric observatory (41.41°S, 174.87°E). Each member of the trajectory ensemble is calculated by offsetting the meteorological data by one meteorological grid point in the horizontal and by 0.01 sigma units in the vertical, resulting in 27 members for all-possible offsets in X, Y, and Z. This method gives a better overview of an air mass' origin compared to that computed for a single particle trajectory.

Because the offset is computed in both directions in the vertical from the starting location, a starting location at the ground would not provide an optimal configuration for this type of simulation (Draxler and Hess, 1998). Furthermore, Draxler and Hess (1998) discovered that the model struggles to recreate accurate trajectories at ground level due to complicating turbulence effects as a result of the interaction of the overlying atmosphere with the surface. Hence, for this type of model run, Draxler and Hess (1998) suggest a minimum starting height of 250m above ground level, significantly higher than the 10m air inlet tower at Baring Head. Given that the physical boundary layer height in the vicinity of New Zealand and the Southern Ocean is approximately 750m (Denning, 2013), I took a trajectory starting height of 500m, between the minimum height required by the model and the top of the PBL. In doing this I assume that air in the physical boundary layer is well mixed and that air arriving at Baring Head at a height of 500m is therefore representative of air arriving at the 10m inlet tower and hence has the same air mass history.

The model computes the 27 particle locations every hour over the period of the 4-day back-trajectory and outputs both a postscript file map projection (Fig 3.5) and a text file containing the latitude and longitude of each particle point, resulting in a total of 2592 particle locations for the 4-day air mass history. These hourly latitude – longitude points are then imported into data analysis software for use with satellite NPP and Argo MLD data.

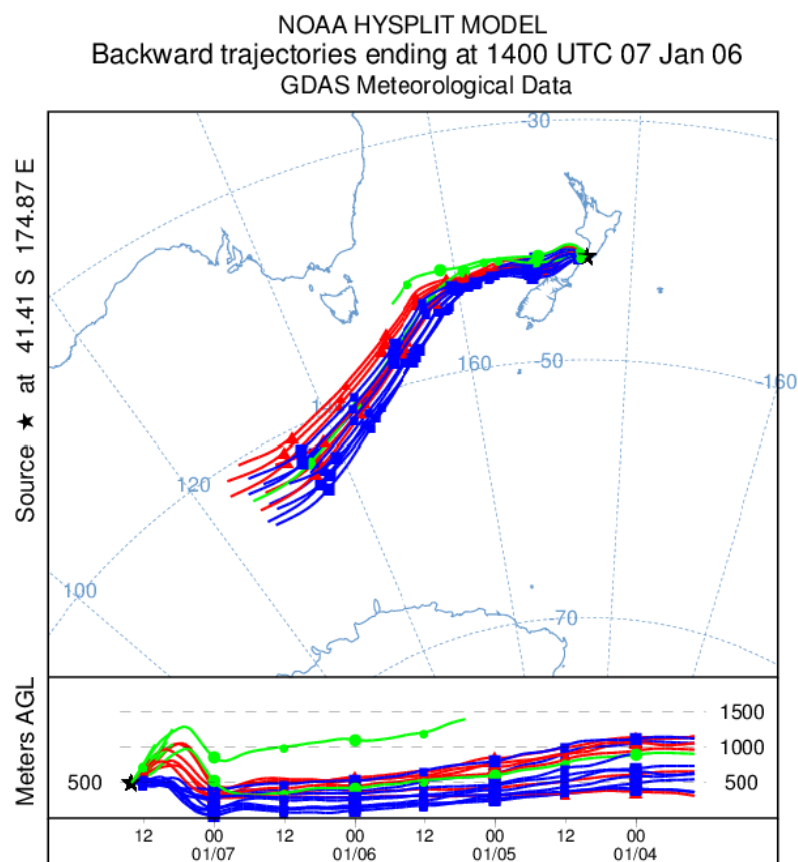


Figure 3.5. Displaying the output generated from the Hysplit\_4 air-mass back trajectory analysis.

### 3.2.4 *Satellite Net Primary Productivity Estimates*

For those events identified as potential primary productivity signals (positive excursions in APO) the 4-day back trajectories were incorporated into global satellite marine net primary productivity (NPP) estimates for the region of influence in order to determine whether the excursion in APO could be reasonably accounted for by observed NPP.

To do this I used data initially collected from the Moderate Resolution Imaging Spectroradiometer (MODIS) instrument on board the Aqua Earth Observing System satellite that was launched in May 2002. Specifically, this instrument estimates surface chlorophyll-a concentration (Chl-a) as a function of measured water leaving radiances. From the surface Chl-a estimates one can then derive NPP. However, to derive this value, further information is needed about the vertical distribution of Chl-a over the depth of the euphotic zone. Here I use the Vertically Generalised Production Model (VGPM) of Behrenfeld and Falkowski (1997) to determine this. The authors' model derives NPP based on Chl-a using a temperature-dependent description of chlorophyll-specific photosynthetic efficiency and is therefore a function of Chl-a, available light, and the photosynthetic efficiency of the phytoplankton. This model, when compared to a global dataset of measured in-situ values of daily integral production, is able to account for 86% of the observed variability (Behrenfeld and Falkowski, 1997). It is therefore a useful tool in deriving estimates of NPP from satellite measurements of Chl-a concentration and has been widely used in studies of this nature (e.g. Lueker, 2004; Yamagishi et al., 2008; Nevison et al., 2012).

The productivity data were downloaded from the Ocean Productivity Data Website run by Oregon State University, U.S. (<http://www.science.oregonstate.edu/ocean.productivity/standard.product.php>). Datasets were downloaded as 8-day averages of NPP at a grid size of 1080x2160 in .hdf format and imported into the SeaWiFS Data Analysis System (SeaDAS) provided by NASA's Ocean Colour Project (<http://seadas.gsfc.nasa.gov/>). For each event the 8-day file was chosen as that covering, or closest to, the preceding 4 days before the event (the time period over which the event signal has been assumed to have been accumulated) (Fig 3.6)

Using the SeaDAS image analysis software the latitude-longitude data points derived from the back-trajectory analysis (a total of 2592 particle locations) were imported and overlaid onto the 8-day average NPP estimate image (Fig 3.7). The software then derived statistical data, including mean, maximum and minimum NPP values over the 2592 particle locations, omitting any data points that occurred on land (Fig 3.8). Both the mean and maximum NPP estimate were recorded for each event (in mg C/m<sup>2</sup>/day). These estimates were then compared to those calculated from the simple air-sea flux model defined in Section 3.2.2.

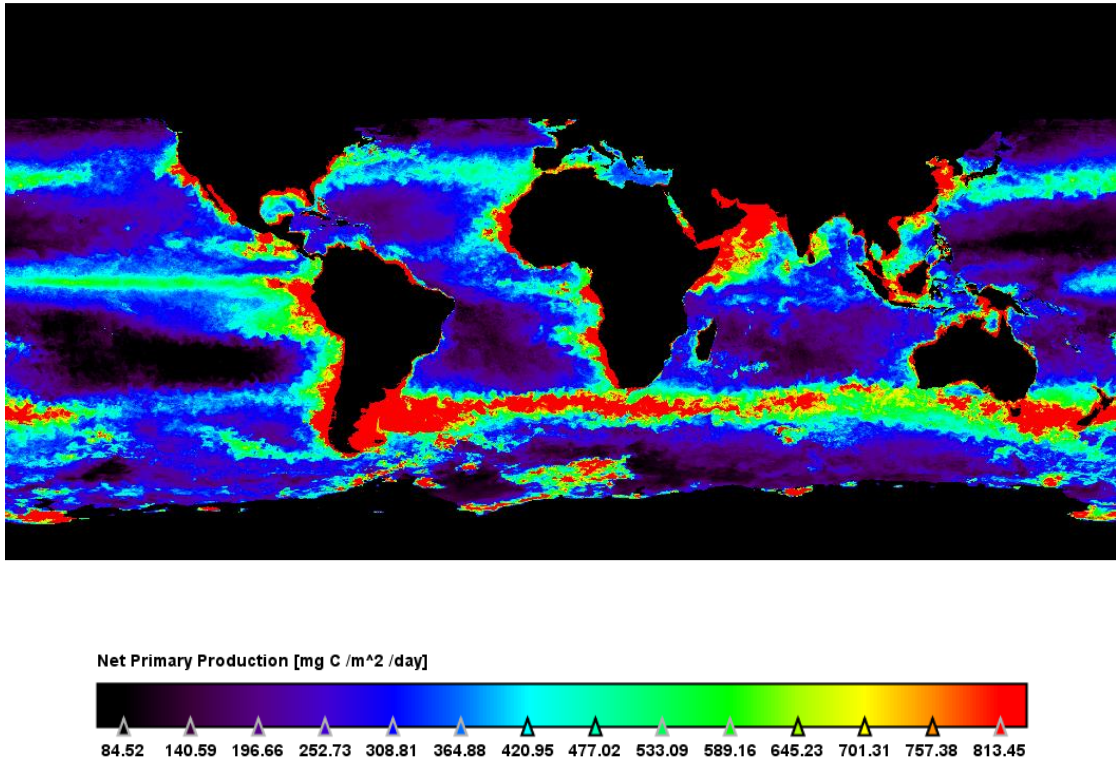


Figure 3.6 Global NPP estimates derived from the VGPM model of Behrenfeld and Falkowski (1997).

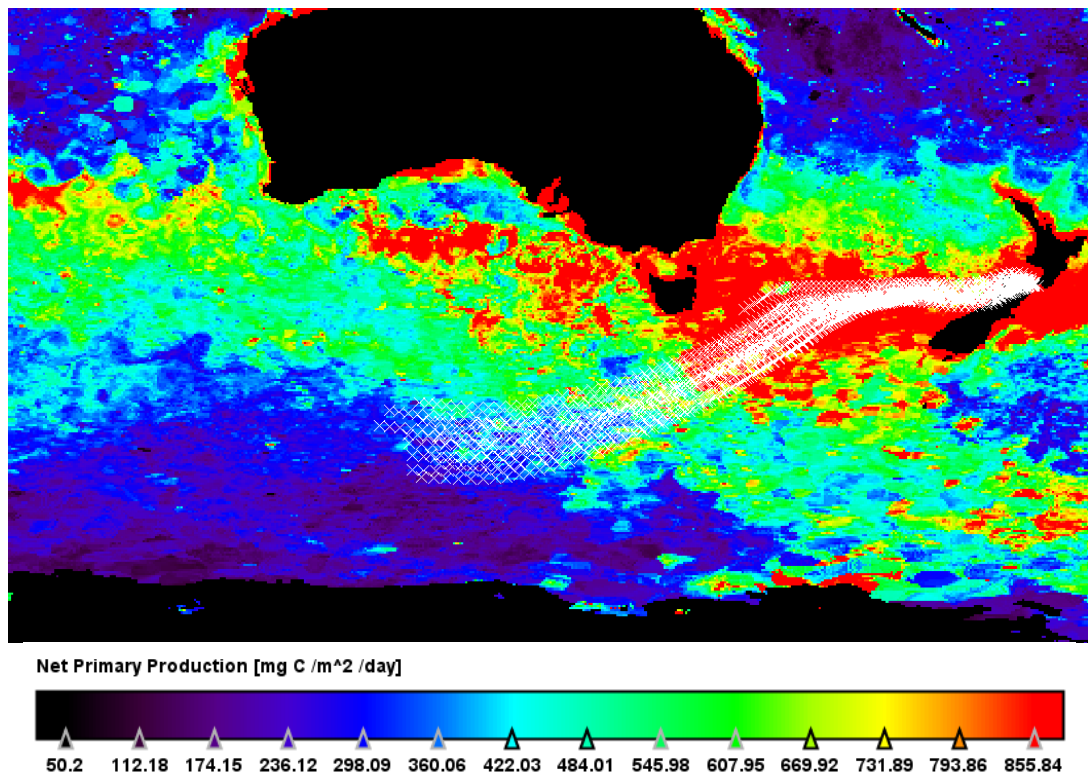


Figure 3.7 Displaying the results of the air mass back trajectory analysis overlaid onto satellite NPP data.

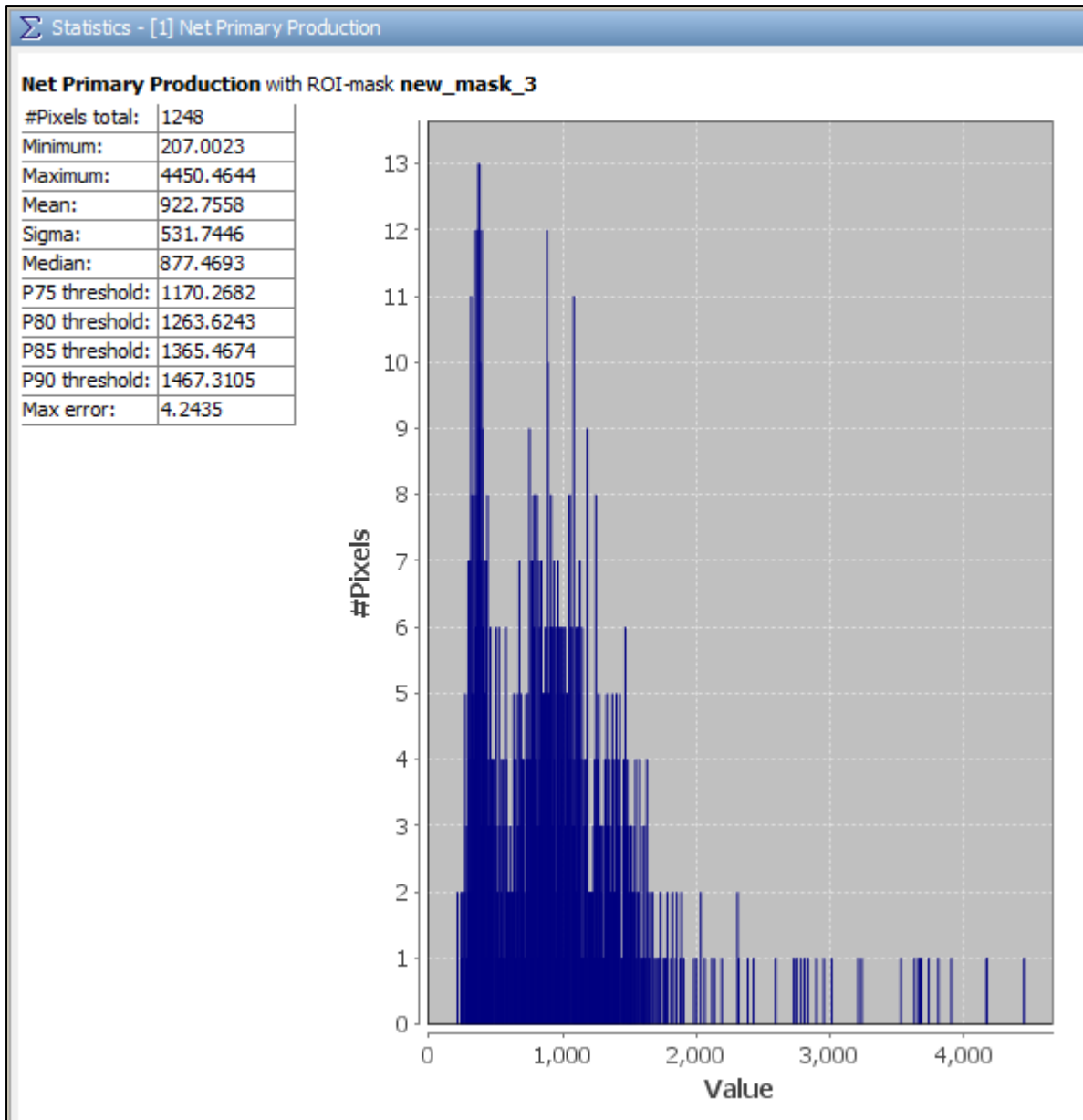


Figure 3.8 Displaying the statistics generated from the satellite NPP image pixels that intersected the air-mass back trajectory analysis results. Data displays NPP in  $\text{mg m}^{-2} \text{day}^{-1}$ .

### 3.2.5 Argo Float Profile Mixed Layer Depth Estimates

For those events identified as potential ventilation signals (negative excursions in APO) the 4-day back trajectories were incorporated into a map projection of MLD. In doing this, I assessed whether the region of influence for the event is characterised by a deep mixed layer and hence is indicative of regions where deep C-rich,  $\text{O}_2$ -poor waters are mixing with surface waters and subsequently exchanging  $\text{CO}_2$  and  $\text{O}_2$  with the overlying atmosphere.

In determining the MLD for a particular region I use data obtained from the Argo float profiling system, launched in 2000. Argo floats measure both temperature and salinity of the water column and therefore allow one to determine the depth of the mixed layer. The dataset used in this study was

provided by the Japan Argo Delayed Mode Data Base ([http://www.jamstec.go.jp/ARGO/argo\\_web/MILAGPV/index\\_e.html](http://www.jamstec.go.jp/ARGO/argo_web/MILAGPV/index_e.html)) of the Japan Agency for Marine-Earth Science and Technology (JAMSTEC) (Hosoda et al., 2010).

As of the 30<sup>th</sup> July, 2013 there are 3525 floats covering the global oceans. Each float descends to a depth of ~1000-2000m (the parking depth) where it then floats freely. Every 10 days the float ascends to the sea-surface making measurements of temperature and salinity as it rises (Dong et al., 2008). The data are then averaged at a resolution of 10m in the top 200m of the water column; below this depth the spacing of the averaging increases linearly to a resolution ~100m at 2000m depth (Dong et al., 2008). At the surface, the data are transmitted to satellites and the Argo float descends and repeats the process.

From the temperature and salinity profiles MLD is calculated as 10-day averages using the threshold finite difference methodology of Hosoda et al., (2010). This method determines the MLD based on threshold criteria of temperature and density where the MLD is defined at the point where either the temperature or the density difference between overlying and underlying water masses is greater than  $\Delta T=0.2^{\circ}\text{C}$  and  $\Delta\sigma\theta=0.03\text{kg/m}^3$  respectively (Hosoda et al., 2010). This method has the advantage of giving both an improved representation of the MLD vertical change due to high vertical resolution and gives a better representation of temporal changes compared to that of monthly averaged Argo data (Hosoda et al., 2010).

For each ventilation event identified, the 10-day average MLD depth data was chosen as that covering all, if not most of the 4-days preceding the start of an event (the time period over which the atmospheric signal is assumed to have been accumulated). The data were imported into the Ocean Data View (ODV) data analysis package, which then projected MLD onto a map of the ocean surrounding New Zealand. Each float profile was then interpolated over a 40 mile radius of the initial data point. The latitude-longitude hourly data points derived from the back-trajectory analysis (a total of 2592 particle locations) were then imported and overlaid onto the 10-day MLD estimates (Fig 3.9). In doing this, an assessment was made as to whether the region of influence defined by the back-trajectory displayed a deep mixed layer. If this were the case then the event signal was presumed to be recording a region where deep C-rich, O<sub>2</sub> deficient waters were upwelling and exchanging with the atmosphere.

### 3.2.6 Dissolved O<sub>2</sub> depth profiles for the Southern Ocean

Dissolved O<sub>2</sub> profiles for the Southern Ocean were downloaded from the World Ocean Atlas, 2009 dataset ([http://odv.awi.de/en/data/ocean/world\\_ocean\\_atlas\\_2009/](http://odv.awi.de/en/data/ocean/world_ocean_atlas_2009/)) (Garcia et al., 2010). The data were downloaded in an ODV-ready format and therefore immediately imported into this data analysis software package. The data are derived from historical oceanographic cruises from around the globe. Data are presented as typical monthly depth profiles across a latitudinal section of the Southern Ocean

and are shown in (Fig 3.10). The  $\Delta pO_2$  estimates were derived from the difference between surface  $pO_2$  and that at the MLD for the latitude of the event defined by air mass back trajectory analysis.

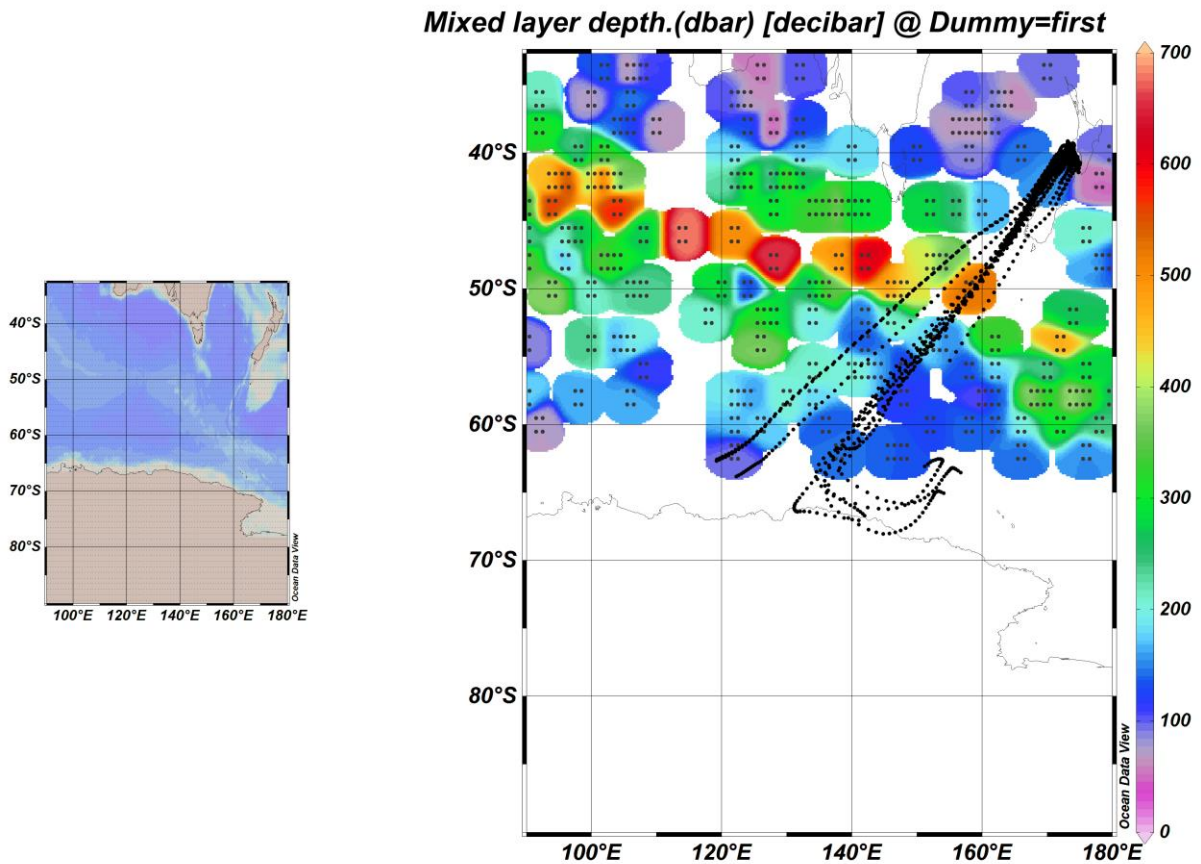


Figure 3.9. The plot on the left displays the region under investigation. The plot on the right displays the MLD at the Argo float profile stations where each station is represented by 4 dots in a square. The air mass back-trajectory is shown by the bold black dots

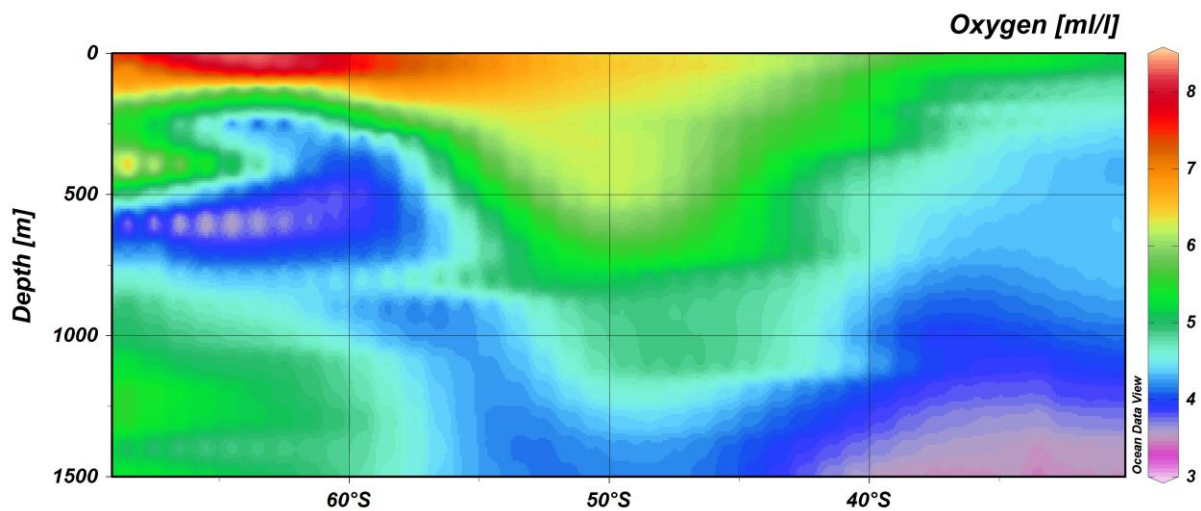


Figure 3.10. Displaying  $pO_2$  depth profiles for a latitudinal section across the Southern Ocean for the month of November.

## 4 Results and Discussion

### 4.1 Introduction

In this section I present the results of my analysis, their interpretation and a discussion of their significance simultaneously. Firstly, I present the atmospheric O<sub>2</sub>, CO<sub>2</sub> and APO observations from Baring Head for the period 1999-2012, including an analysis of the overall trends observed in the data, the seasonal variation of CO<sub>2</sub> and O<sub>2</sub> and the inter-annual variability of APO, which is compared to the SAM and ENSO indices. I then go on to discuss the characteristics of the carbon cycle events identified in the study period, including their annual, monthly and seasonal distribution, the magnitude of APO change recorded over the event periods and the O<sub>2</sub>:CO<sub>2</sub> exchange ratios. Following this, I present the results from the conceptual model defined in Section 3.2.2 and discuss its limitations. I will end this section by presenting two events, one for NPP and ventilation, respectively, with a full work up of the data that fed into my conceptual model, including the air-mass back-trajectory analysis, satellite NPP estimates and pO<sub>2</sub> concentrations displayed at the MLD. In my interpretation of the results I try to compare, where possible, to peer-reviewed literature. However, this is not possible for the majority of my results since the methodology developed here is unique. Furthermore, I am analysing unpublished atmospheric O<sub>2</sub> and APO data and as such my results represent the first presentation of these observations.

### 4.2 Atmospheric O<sub>2</sub>, CO<sub>2</sub> and APO Observations 1999-2012

#### 4.2.1 General Trends

The atmospheric O<sub>2</sub>, CO<sub>2</sub> and APO observations for the study period, 1999-2012, are shown in Fig 4.1. The ‘clean up’ of this dataset is an ongoing process within my supervisor’s research group and as such, there are still a few time periods where erroneous values are still present, such as those centred around 2005 and towards the beginning of 2009. 2005 was a particularly bad year for data collection with regards to O<sub>2</sub> measurements due problems with the air inlet tower (A. Manning, personal communication). Subsequently, this year was omitted from the event identification aspect of this project.

Through inspection of Fig 4.1, one can clearly discern an increasing trend in CO<sub>2</sub> concentrations over the study period and a decreasing trend in both O<sub>2</sub> and APO concentrations. Furthermore, O<sub>2</sub> and APO display a clear seasonal cycle in comparison to CO<sub>2</sub>, which displays a smaller, less obvious seasonal cycle.

To examine the O<sub>2</sub>, CO<sub>2</sub> and APO data in more detail the results were fed into the curve fitting program Hpspline (See Section 3.1.2) to decompose the observed signal into its constituent components, that is the deseasonalised trend (Fig 4.2), the detrended seasonal component (Fig 4.3A-

C) and the detrended, deseasonalised component (Fig 4.3D-F) which represents the inter-annual variability of the respective species.

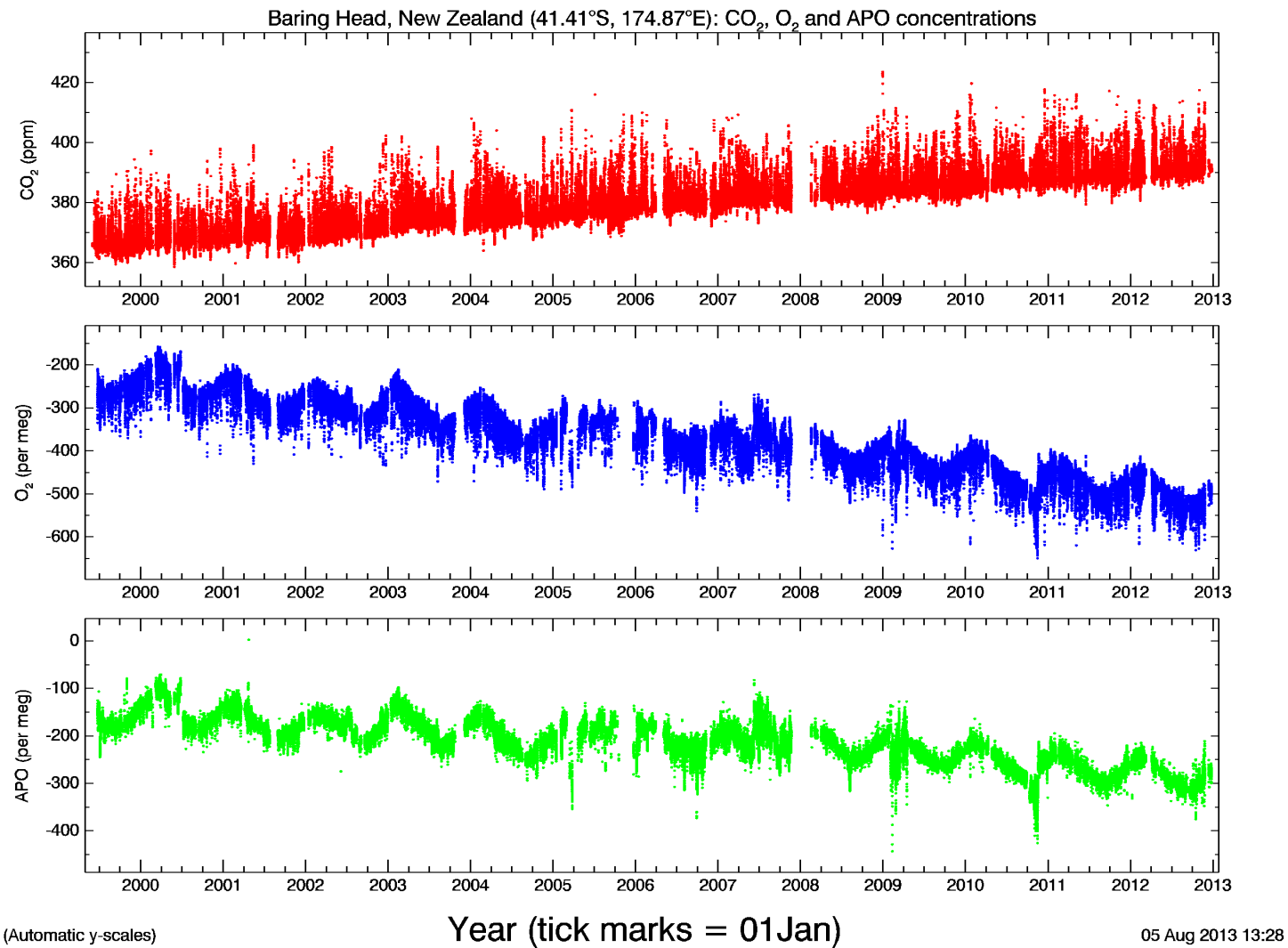


**Figure 4.1.** The full atmospheric observation record of CO<sub>2</sub> (red points), O<sub>2</sub> (blue points) and APO (green points) from July 1999 through to the end of 2012, at Baring Head, New Zealand.

CO<sub>2</sub> concentrations increased from a value of 367.1 ppm in July 1999 to 391.5 ppm in July 2012, corresponding to an average atmospheric growth rate of 1.9 ppm yr<sup>-1</sup> and equivalent to the addition of 4.0 Pg C yr<sup>-1</sup> (assuming a molar mass for carbon of 12.0 g mol<sup>-1</sup>, and the total moles of air in the atmosphere = 1.77 x 10<sup>20</sup> mols). Over the same time period, the average carbon emissions from fossil fuel burning, cement manufacture and gas flaring were 8.1 Pg C yr<sup>-1</sup>, (Boden and Andres, 2013). Following the methods and assumptions of Manning and Keeling (2006), specifically using equations 10 and 12 from their paper, I calculate the global terrestrial and oceanic carbon sinks using the rate of APO decline from my data (-11.2 per meg yr<sup>-1</sup>). The oceanic and terrestrial carbon sinks were found to be 2.2 Pg C yr<sup>-1</sup> and 1.9 Pg C yr<sup>-1</sup>, respectively for the 1999-2012 study period.

#### 4.2.2 *Seasonal variability*

The seasonal variability of CO<sub>2</sub>, O<sub>2</sub> and APO are displayed in Fig 4.3A-C. The amplitude of the seasonal cycle for CO<sub>2</sub> is 0.9 ppm, whereas for O<sub>2</sub> it is 54 per meg. The seasonal amplitude of CO<sub>2</sub> is influenced by seasonal gas exchange between the terrestrial biosphere and the atmosphere and between the oceans and the atmosphere (Keeling and Shertz, 1992). This signal is largely driven by the Northern Hemisphere terrestrial biosphere, which, given the ~ 6-month mixing time between hemispheres acts to reinforce the small terrestrial biosphere signal of the Southern Hemisphere. Photosynthesis dominates the signal during the southern hemisphere spring and summer months, absorbing CO<sub>2</sub>, driving CO<sub>2</sub> concentrations down and emitting O<sub>2</sub>, driving O<sub>2</sub> concentrations up. Respiration dominates in the southern hemisphere autumn and winter months, releasing CO<sub>2</sub> and consuming O<sub>2</sub>. In addition to the terrestrial biosphere signal, the O<sub>2</sub> seasonal cycle is also influenced by seasonal gas exchange with the oceans driven by NPP and the seasonal breakdown of the thermocline, allowing mixing and ventilation of O<sub>2</sub> deficient waters (Keeling and Shertz, 1992). This component is captured by the seasonal APO cycle (amplitude = 54 per meg) which, by definition, is conservative to terrestrial biosphere process (Stephens et al., 1998).

#### 4.2.3 *The inter-annual variability of APO*

As set out in WP1, one of the aims of this study was to investigate the inter-annual variability in APO and determine whether any of the variability can be explained by correlation with the climate indices for the SAM and ENSO. Although an analysis of CO<sub>2</sub> and O<sub>2</sub> inter-annual variability was beyond the scope of this study, they are included in Fig 4.3 for completeness. An analysis of these data is planned in the follow up work to my thesis.

##### 4.2.3.1 *Main features of the data*

Fig 4.3F displays the inter-annual variability in APO. The most prominent feature of the inter-annual variability is the large decline in APO (~125 per meg) during 2005. As discussed Section 4.2.1 this year was a particularly bad year for data collection due to issues with air inlet tower that resulted in O<sub>2</sub> observations reported well below what was expected for the general O<sub>2</sub> trend. Hence, this feature can be ignored since it is not related to carbon cycle processes.

Other prominent features in the data indicate relatively large increases in APO (~40-50 per meg) during 2000, 2004 and 2007. These features are presumed to reflect increases in NPP during the years mentioned, since higher NPP will result in an increase in the O<sub>2</sub> flux out of the ocean, leading to a corresponding increase in APO. In the subsequent analysis of WP2, I will seek to confirm this hypothesis by examining whether there is either an increase in the number of NPP events recorded or an increase in the magnitude of APO change recorded over the event period in these particular years.

Furthermore, Fig.4.3F displays three prominent decreases in APO (~40-60 per meg) during 2003, the beginning of 2006 and the beginning of 2009. These features are presumed to reflect an increase in the ventilation of deep water masses depleted in O<sub>2</sub> and so driving a flux of O<sub>2</sub> into the ocean from the atmosphere leading to a corresponding decrease in APO. Again, I will examine this hypothesis in WP2 by examining whether there is an increase in the number of ventilation events recorded, or whether there is an increase in the magnitude of APO change recorded over the event period.

#### 4.2.3.2 *APO inter-annual variability and the SAM and ENSO indices*

The results of the comparison of the APO inter-annual variability with the climate indices of the SAM and ENSO are displayed in Fig 4.4. I found no correlation between the data. This is in contrast to the study presented by Verdy et al., (2007) who concluded, based on their own physical-biogeochemical model of air-sea gas exchange, that a significant proportion of the inter-annual variability of air-sea O<sub>2</sub> fluxes within the Southern Ocean can be explained by the SAM and ENSO. Hence, by deduction the indices should also correlate with APO variability. The discrepancy between their model results and my atmospheric observations may be partly explained by the different time periods of study, although there is a 5-year period of overlap. Furthermore, the results of Verdy et al., (2007) will be influenced by their model parameterizations, which may not represent real-world processes correctly. Additionally, my results are sensitive to the choice of curve-fitting program used on the atmospheric data (Hpspline) (Pickers, 2013) and in the choice of the SAM and ENSO indices which are defined slightly differently by different authors and research groups (Wallace and Thompson, 2002). Therefore in the planned follow up work to this project, I intend to investigate the sensitivity of my data to different curve-fitting procedures and also to different climate indices datasets.

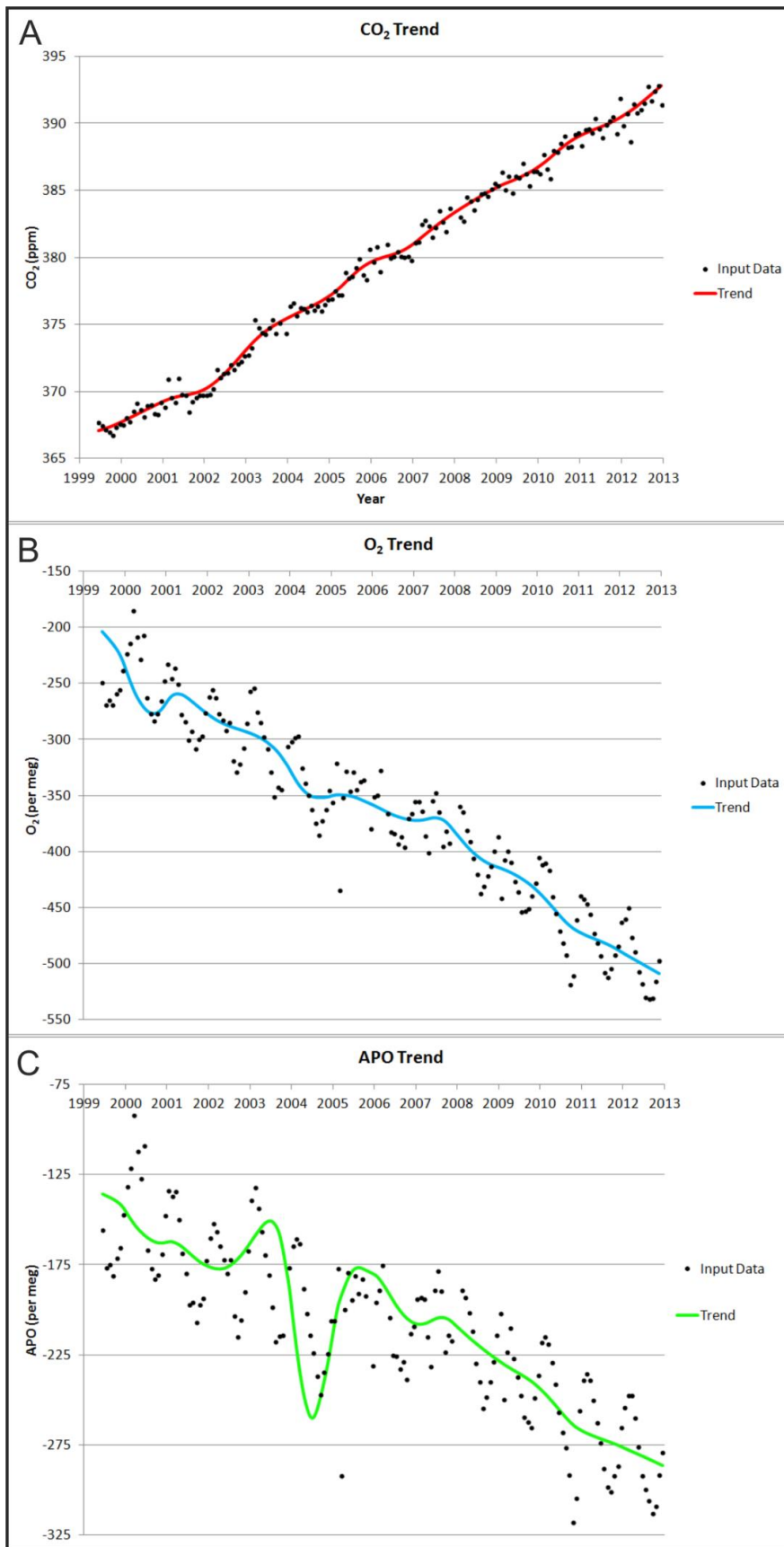
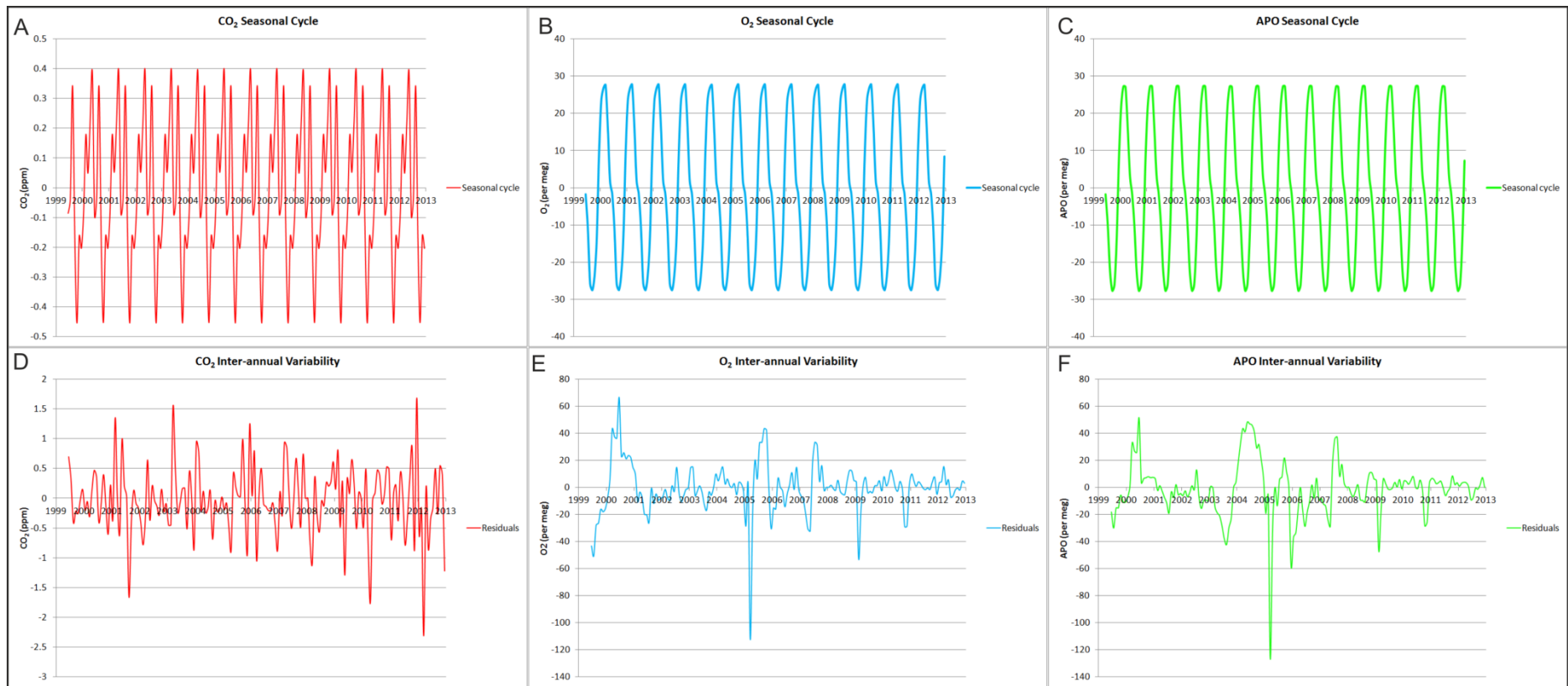


Figure 4.2. Results from the Hpspline curve-fitting procedure displaying the overall trend in the CO<sub>2</sub> (A), O<sub>2</sub> (B), and APO (C) observations for the study periods, 1999-2012. Input data represents the monthly means of the atmospheric concentrations.



**Figure 4.3. Results from the Hpspline curve-fitting procedure displaying firstly the de-trended, seasonal component of the CO<sub>2</sub> (A), O<sub>2</sub> (B) and APO (C) observations, and secondly, the de-trended, de-seasonalised component for CO<sub>2</sub> (D), O<sub>2</sub> (E) and APO (F) representing the inter-annual variability in these species.**

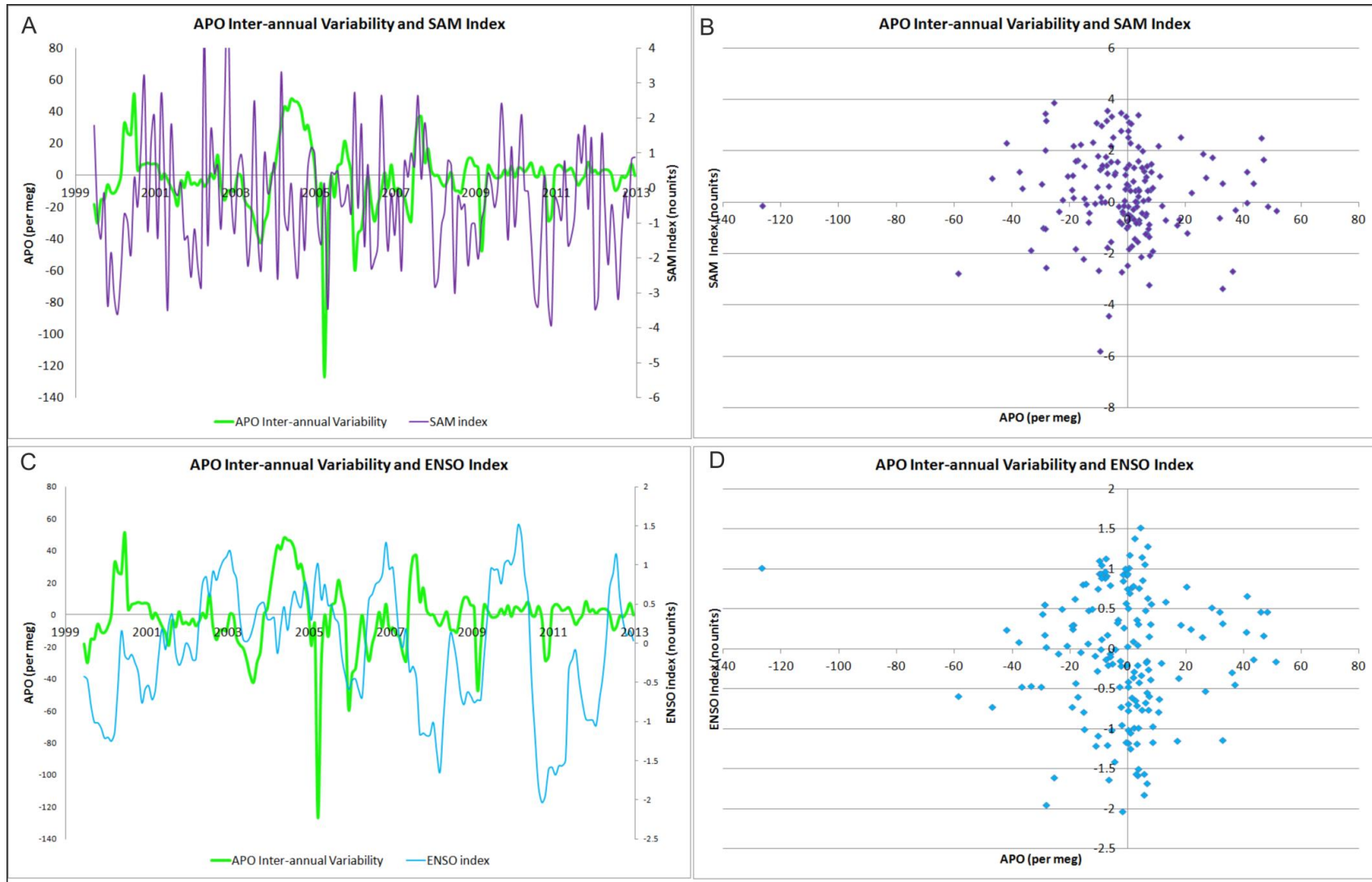


Figure 4.4. Results of the comparison of APO inter-annual variability with the SAM (A and B) and ENSO (C and D) climate indices. Results are presented as a time-series in A and C and as correlative plot in B and D.

### 4.3 Identifying NPP and ventilation events from atmospheric observations

#### 4.3.1 Annual variability of identified events

A total of 78 events were identified throughout the 1999-2012 period (Fig 4.5), corresponding to an average of 6 recorded events per year. However, the recorded events were not evenly distributed throughout the study period as displayed in Fig 4.6A. For example, in 2007, 21 events were recorded, the most of any year within the study period. This contrasts with the following year (2008) when only one event was identified. Consequently, when attempting to interpret the data for the whole study period, some years will have a greater influence on the final result compared to others and therefore caution must be taken when drawing conclusions about the full dataset. As such, a year with a particularly large number of events recorded does not necessarily mean that oceanic carbon cycle processes within the vicinity of Baring Head were more active during this period, although this is one interpretation, but rather that more events were *recorded* and may therefore be down to more favourable identification conditions.

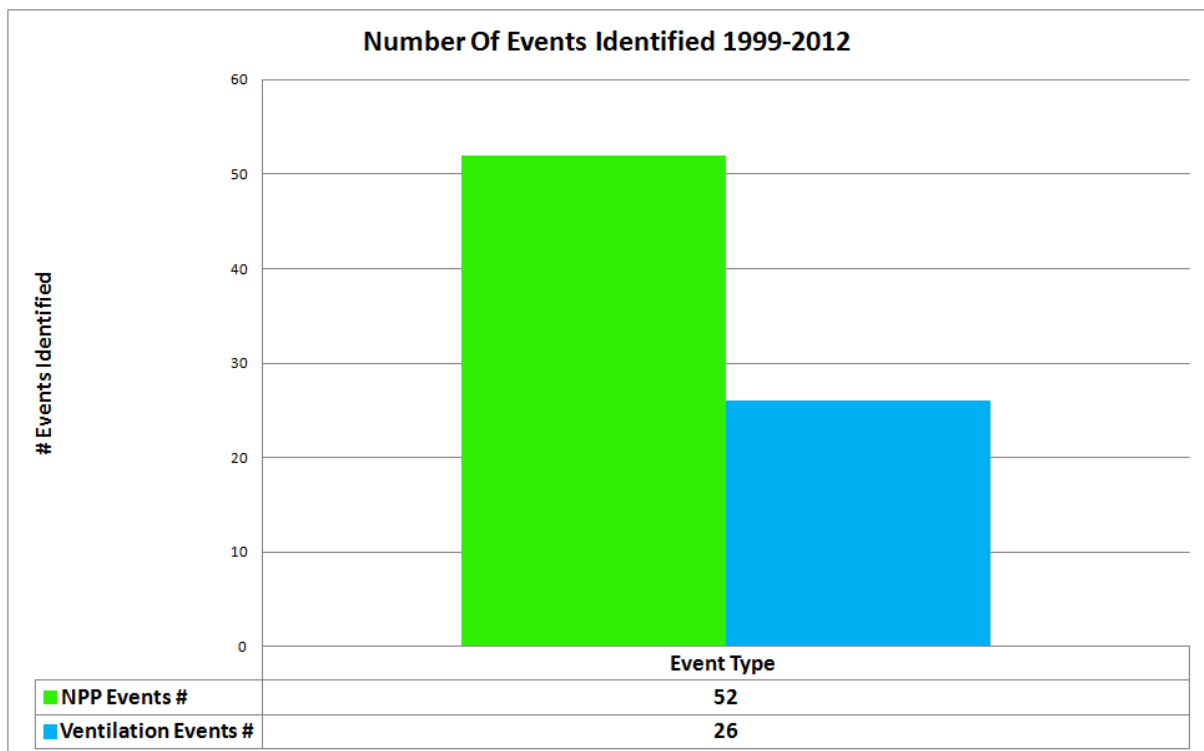
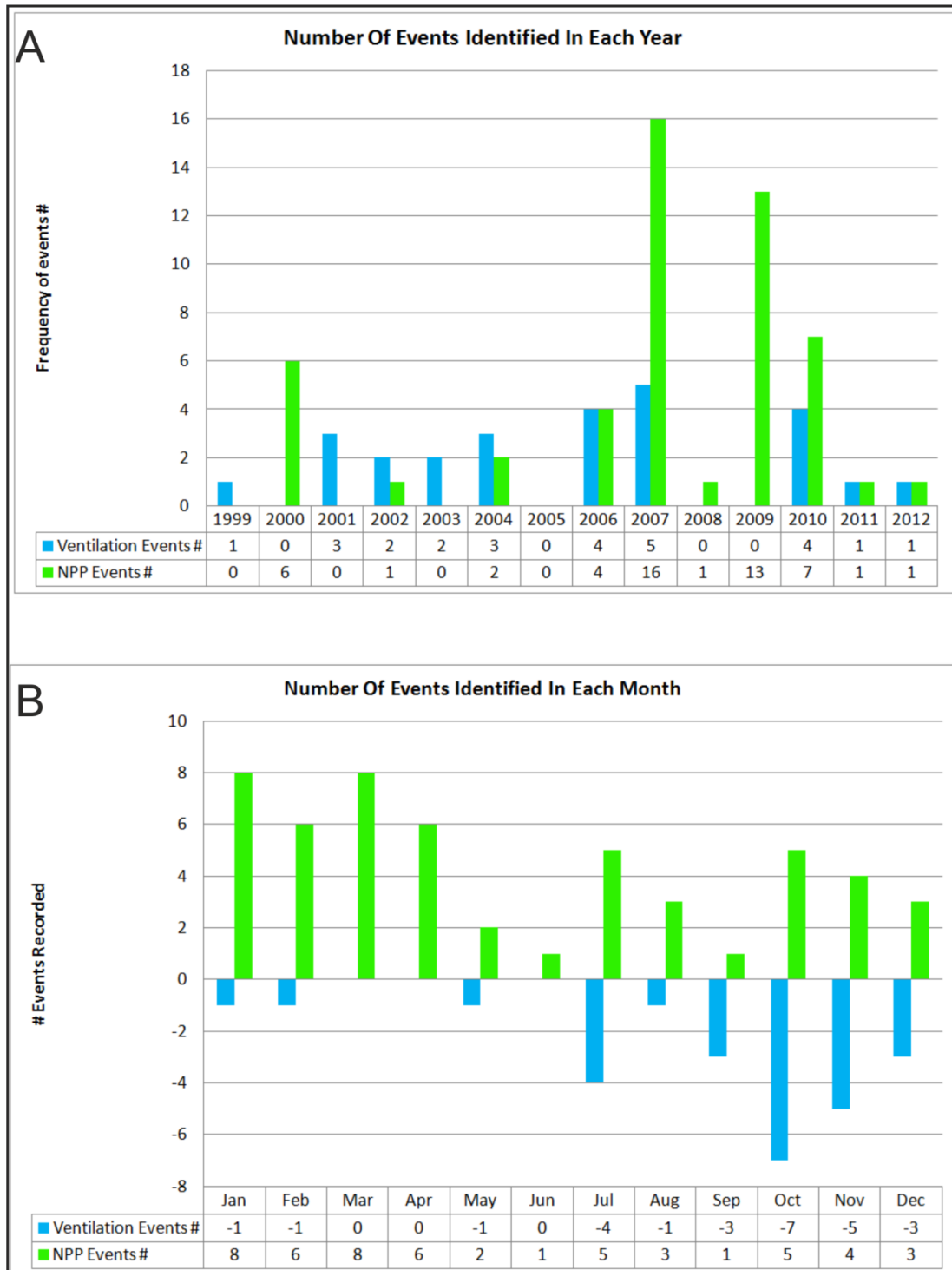


Figure 4.5 Total number of NPP (green) and ventilation (blue) events identified in the study period (1999-2012).

The number of events recorded that were assumed to be reflecting NPP (52 events) were twice that of those assumed to be reflecting ventilation (26 events) (Fig 4.5) I interpret this to indicate that the atmospheric O<sub>2</sub> and CO<sub>2</sub> observations at BHD are more greatly influenced by regions of NPP than regions of ventilation. This reflects the closer proximity of BHD to regions of the Southern Ocean where NPP is high (30°S) compared to regions of ventilation (50°S) (Takahashi et al., 2012). Furthermore, Nevison et al., (2005) showed that the seasonal cycle of O<sub>2</sub> at Cape Grim, Tasmania,

after removing the terrestrial biosphere component, is more influenced by NPP than it is by ventilation of O<sub>2</sub> poor deep waters. Therefore, given the proximity of BHD to Cape Grim, one would expect a stronger NPP signal in the APO observations.



**Figure 4.6.** Frequency of NPP events (green) and ventilation events (blue) identified by year (A) and by month (B). In plot B, the frequency of events is displayed as a positive number for NPP events to represent the increase in APO over the event period and displayed as a negative number for ventilation events to represent a decrease in APO over the event period.

One of the major difficulties in identifying events was the variability of the wind direction at BHD. Fig 4.7 shows that ~56% of air arriving at BHD is from a northerly direction 340-40°, with air having to cross the North Island before reaching BHD and will therefore be influenced by gas exchange with the terrestrial biosphere. Only 35% of the winds arrive from a southerly direction (120-210°), which from the point of view of identifying events, means that only 35% of the record is sampling clean ocean air originating from the Southern Ocean. Nonetheless, the distribution of wind directions did vary from year to year and as such, some years were more favourable to event identification due to air masses originating more frequently from areas of the ocean. For example in 2007, the year with the most events identified (21), wind distributions displayed an increase in the frequency of winds arriving from 270-360° which covers the area of the Tasman Sea (19%) compared to the full dataset (11%). Whereas for 2008, when only one event was identified the majority of the winds (36%) came from 0-20°, deriving from the North Island and had a higher occurrence of carbon cycle events relating to terrestrial biosphere gas exchange.

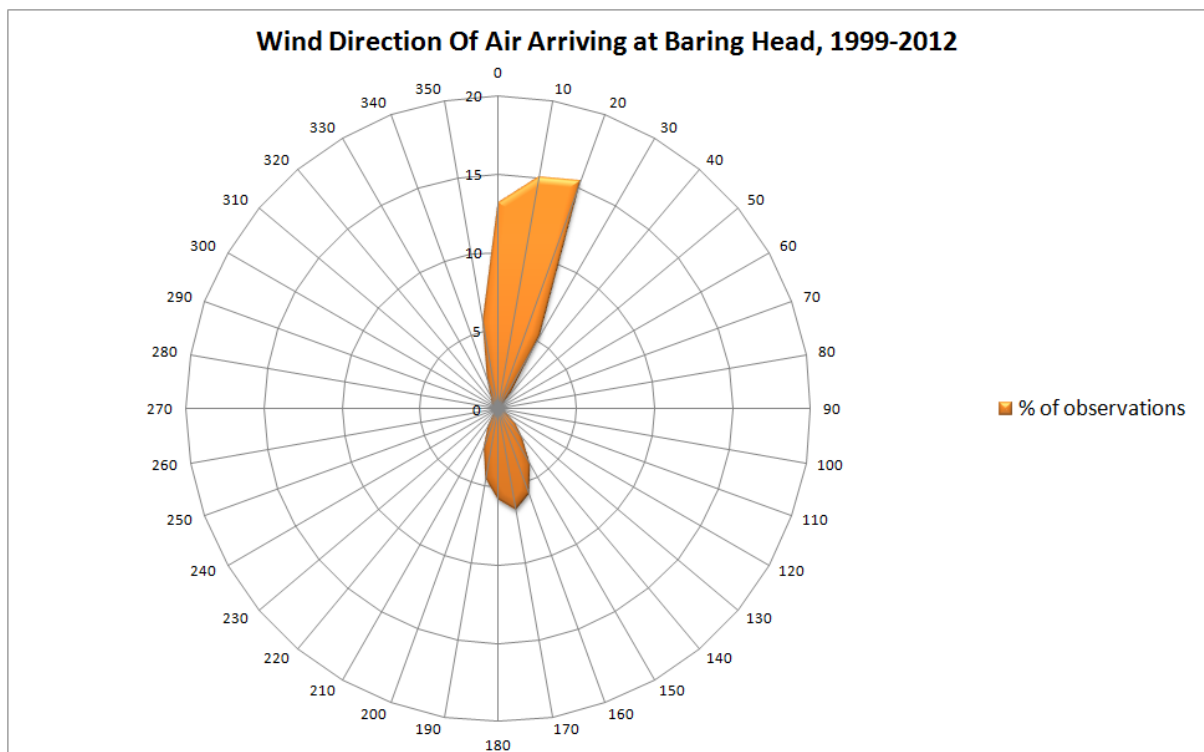


**Figure 4.7. Wind direction of air arriving at Baring Head for the period 1999-2012. Wind direction is displayed in degrees (°) and the frequency from each 10° bin is displayed as a percentage.**

The inter-annual variability of APO (Fig 4.3F) suggested that NPP in 2007 was particularly productive. As shown in Fig 4.6A, 2007 was the year with the most NPP events identified (16) and, considering that more air was being sampled from the Tasman Sea, a particularly productive region of the ocean surrounding New Zealand (Baird et al., 2008), this appears to explain the increase in APO observed in this year. However, the inter-annual variability of APO did not display any peaks in 2009 and 2010, the second and third most frequent NPP event identification years, and so caution must be

taken with the above interpretation for NPP event frequency in 2007. Additionally, there is no indication in the ventilation event frequency that can explain the troughs in the APO inter-annual variability in 2003, 2006 and 2009. There is a relatively even spread in the ventilation events identified across the study period with 2006, 2007, 2010 displaying the most identified events. However, given the small sample size of ventilation events (26) it is perhaps not surprising that the inter-annual variability in APO is not captured.

#### *4.3.2 Monthly and seasonal variability of identified events*

Fig 4.6B displays the frequency of the respective event types recorded in each month of the year. In contrast to the results for events recorded by year, no sampling bias is thought to exist for those recorded by month. Although sampling conditions conducive to event identification may be variable between the same months of different years and from month to month of the same year (due to the variability of winds deriving from oceanic regions), the results presented by month are averaged over the full 13 year dataset and so it is presumed that any sampling bias is negligible. As such, the frequency of a particular event in a particular month is assumed to represent true seasonal variations in oceanic carbon cycle event activity. However, a bias is introduced by the fact that twice the number of NPP events were recorded compared to ventilation events and hence the seasonal variation is better represented in the NPP events compared to ventilation events.

The highest number of NPP events were recorded in January and March (8 events each) and the lowest in June and September (1 event each). The highest numbers of ventilation events were recorded in October (7 events). No ventilation events were found in March, April or June. Again, this distribution may be reflecting the deficiency in the number of ventilation events found. The lowest number of events identified for both event types were recorded in June. This may reflect the fact that this time period is during the southern hemisphere winter and thus light available for photosynthesis will be low. Furthermore, sea-ice around Antarctica begins to form during this period (Takahashi et al., 2012) potentially covering regions of ventilation and therefore suppressing air-sea gas exchange. Furthermore, there is an increase in the number NPP events recorded between September and October. This could plausibly be driven by the spring phytoplankton bloom due to both an increase in light availability and in the nutrients supplied by mixing of deep water with surface waters during the previous winter. The ventilation signal is consistent with this interpretation (highest number of events recorded between September and November), and although mixing is assumed to occur in the winter, air-sea exchange does not occur until the spring due to the persistence of the sea-ice barrier (Takahashi et al., 2012).

To investigate the seasonal variability further, I binned the number of events identified into 3 month seasonal bins, whereby December-January-February (DJF) represents the southern hemisphere summer, March-April-May (MAM) represents autumn and so on (Fig 4.8A). I took the mean

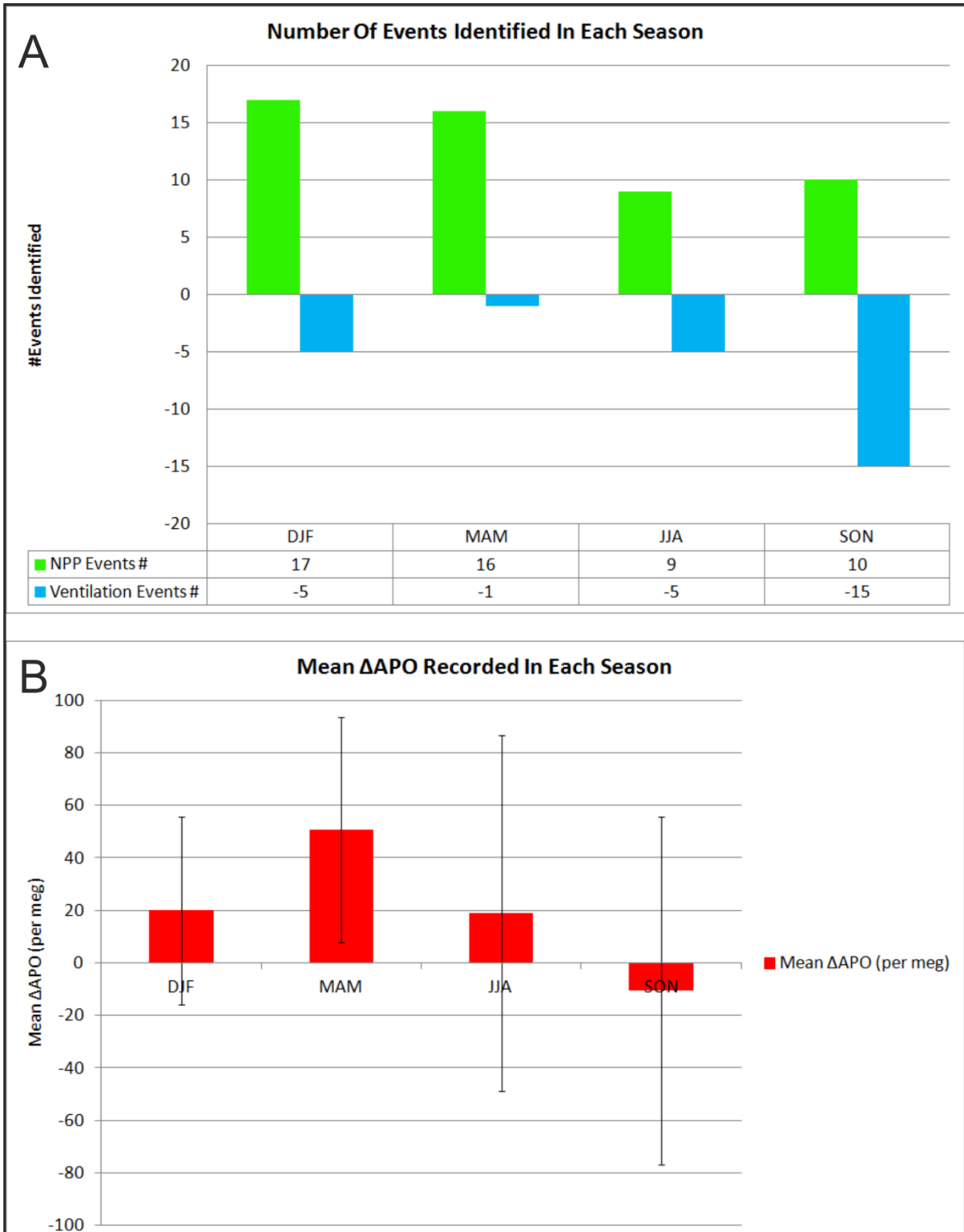


Figure 4.8. Frequency of events identified by season (A) and the mean  $\Delta$ APO of all events identified by their respective season (B). Error bars in plot B represent 1 standard deviation of the sample means. Seasons are defined by 3 month bins where DJF = summer, MAM = autumn, JJA = winter and SON = spring.

magnitude of APO change over the duration of the event periods ( $\Delta APO$ ) recorded in each season, where positive values indicate NPP and negative values indicate ventilation. The highest number of NPP events were recorded in the summer months (DJF) (n=17) whilst the lowest were found in the winter months (JJA) (n=9). This is consistent with the seasonal cycle of NPP within the region (Nevison et al., 2005). The highest number of ventilation events were recorded in the spring months (SON) (n = 15) whereas the lowest number of events were found in the autumn months (MAM) (n = 1). This also agrees well with the ventilation seasonal cycle in the Southern Ocean derived from N<sub>2</sub>O measurements made by Nevison et al., (2005).

To determine the significance in the difference between the mean  $\Delta APO$  for each season I performed a two-tailed statistical t-test, assuming unequal sample variances. The results for each season versus another are shown in Table 4.1. The most significant difference, at the 99% confidence level, was found between MAM (autumn) and SON (spring) (P = 0.001; <0.01). This further corroborates the fact that both the event frequency and event  $\Delta APO$  magnitude recorded in each month represent the seasonal cycle in APO that typically shows a peak in late summer, early autumn and a trough in late winter early spring for the southern hemisphere (Nevison et al., 2005).

**Table 4.1. Results from the two-tailed statistical t- test, assuming unequal variances. The seasons are represented by 3 month bins where DJF = summer, MAM = autumn, JJA = winter and SON = spring.**

<i>Season</i>	<b>MAM</b>	<b>JJA</b>	<b>SON</b>
<b>DJF</b>	P = 0.023	P = 0.963	P = 0.053
<b>MAM</b>	NA	P = 0.144	P = 0.001
<b>JJA</b>	NA	NA	P = 0.199

#### **4.4 Characterising NPP and ventilation events**

##### *4.4.1 Magnitude of APO change ( $\Delta APO$ )*

When seeking to characterise the carbon cycle events under investigation I decided to investigate whether the events recorded displayed a typical  $\Delta APO$ . The results are displayed in Fig 4.9A. Both NPP and ventilation events displayed similar values for the mean and standard deviation of  $\Delta APO$ :  $50.1 \pm 33.9$  and  $49.7 \pm 34.0$  per meg respectively. The total range of  $\Delta APO$  recorded was 2.8 to 149.6 per meg for NPP, whereas for ventilation, values ranged between 11.4 and 164.0 per meg. The fact that the mean  $\Delta APO$  for both NPP and ventilation are ~50 per meg is an interesting result since it opens up the opportunity to develop a programming routine that automatically selects for events. However, the magnitude of  $\Delta APO$  is controlled by the event duration, which is typically influenced by the variability of the wind direction of air arriving at the site.

A more convenient metric to characterise the carbon cycle events, therefore, is by the rate of APO change over the event period ( $\Delta APO/t$ ) (Fig 4.9B). The rate of APO change is more directly related to

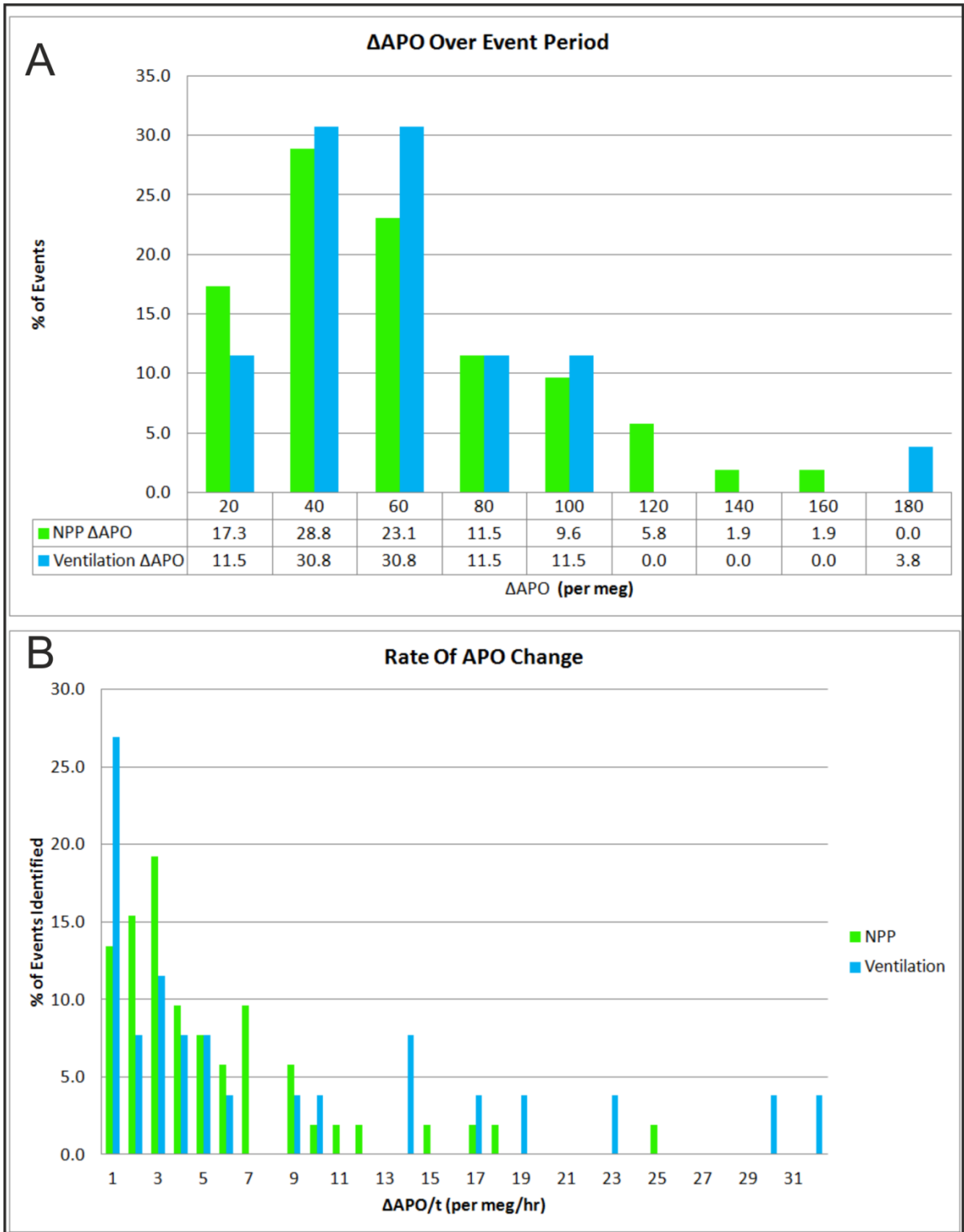


Figure 4.9 Magnitude of APO change ( $\Delta$ APO) over event period (A) and the rate of APO change ( $\Delta$ APO/t) found in each event (B).

the dissolved O<sub>2</sub> concentration within the ocean, whereby high pO<sub>2</sub> concentrations would drive an increase in the rate of APO change compared to that of low dissolved O<sub>2</sub> concentrations (assuming a constant wind speed and therefore gas transfer velocity (Wanninkhof, 1992)).

The most common  $\Delta$ APO/t value for ventilation events was <1 per meg/hr, accounting for 26.9% of the events recorded with a range between 0.1 and 31.4 per meg hr<sup>-1</sup> (Fig 4.9B). NPP events on the other hand, displayed a typical  $\Delta$ APO/t value of between 2 and 3 per meg/hr accounting for 19.2% of the events recorded, with a range between 0.2 and 24.7 per meg hr<sup>-1</sup>.

I believe the difference in the  $\Delta$ APO/t between the two event types reflects the differing spatial scales for gas exchange between the ocean and atmosphere for the respective carbon cycle processes. NPP is focused in the euphotic layer of the ocean, typically in the top 100-200m. O<sub>2</sub> produced as a result of NPP will therefore be concentrated in the euphotic zone and will thus drive a relatively large flux of O<sub>2</sub> to the atmosphere. Conversely, mixing and ventilation of deep water masses occurs over the full MLD, which can vary between 0 and 1500 m. Hence, a decrease in O<sub>2</sub> driven by ventilation of deep water masses will occur over a larger depth compared to changes in dissolved O<sub>2</sub> driven by NPP. The relative flux of O<sub>2</sub> into the ocean from the atmosphere will therefore be less for ventilation compared to NPP.

#### 4.4.2 O<sub>2</sub>:CO<sub>2</sub> molar exchange ratio.

One of the primary aims of this study was to determine whether a common O<sub>2</sub>:CO<sub>2</sub> gas exchange ratio could be found for gas fluxes between the ocean and atmosphere driven by NPP and ventilation. If a common exchange ratio could be found then it would aid in the identification of carbon cycle events found in other atmospheric O<sub>2</sub> and CO<sub>2</sub> observations from across the globe.

Fig 4.10A displays the full range of O<sub>2</sub>:CO<sub>2</sub> ratios found in this study. Since the exchange of O<sub>2</sub> and CO<sub>2</sub> are presumed to be occurring in opposite directions, the exchange ratio should be negative. However, as shown by Fig 4.10A, many of the events recorded display positive values as a result of O<sub>2</sub> and CO<sub>2</sub> changes occurring in the same direction. This result is not surprising however, since the exchange time for CO<sub>2</sub> between the atmosphere is much slower than that for O<sub>2</sub> (Broecker and Peng, 1982; Keeling, 1988; Bender and Battle, 1999) and so over these short event periods (hours to days) the O<sub>2</sub> and CO<sub>2</sub> exchange becomes uncoupled. Hence, the CO<sub>2</sub> change recorded over the event period is not necessarily reflecting changes due to carbon cycle process.

Fig 4.10A shows that the majority of events display a ratio between -20 and 20. I therefore examined this sub-population further for each respective event type and further converted all ratio values to positive numbers to determine if a common exchange ratio could be found for each particular event type (Fig 4.10B). For NPP, the largest number of events (9) displayed a ratio between 2 and 4, with a mean for this sub-population of  $6.8 \pm 4.3$  and with a range between 0.7 and 19.1. Whereas for

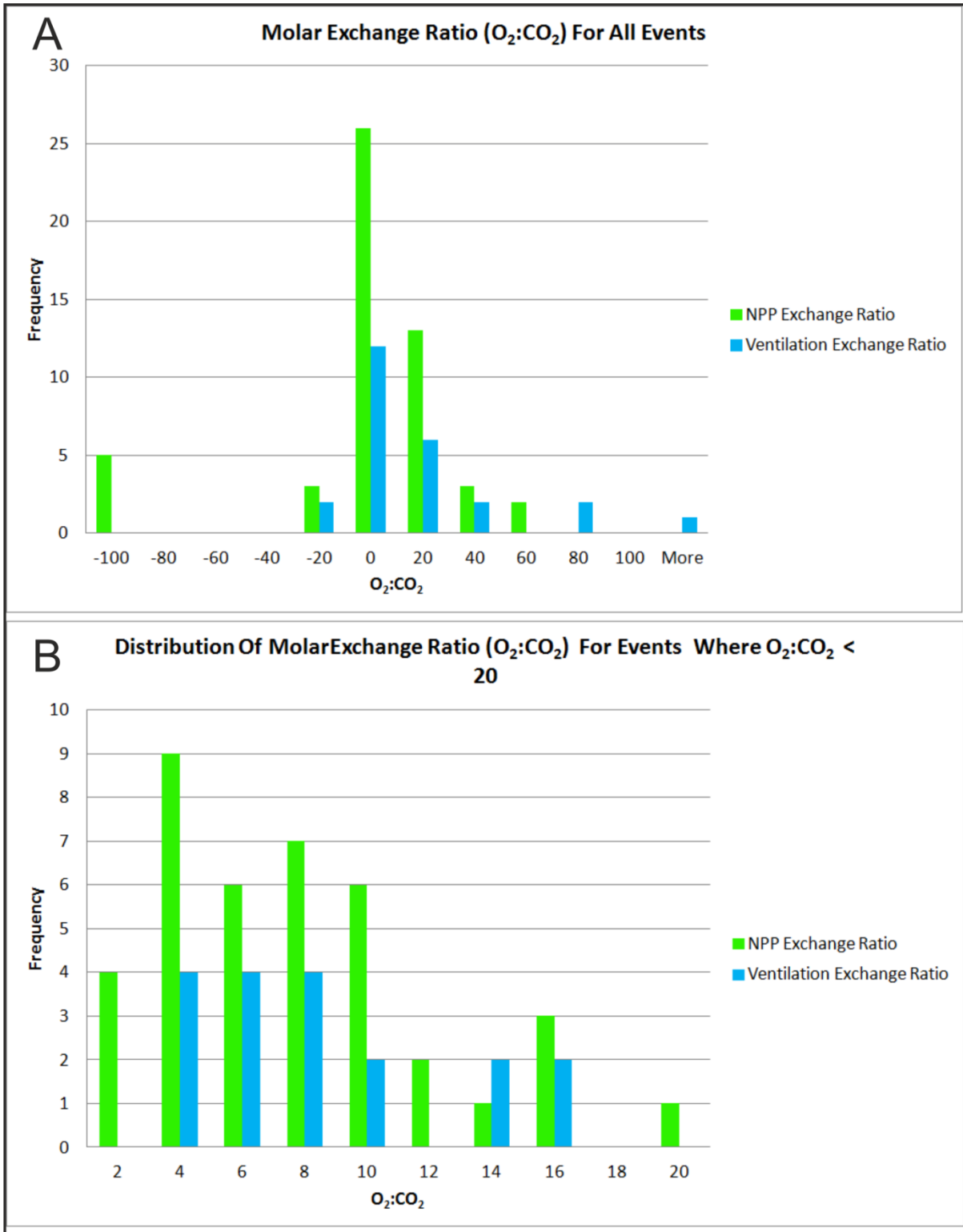


Figure 4.10. The molar exchange ratio ( $O_2:CO_2$ ) for all events identified within the 1999-2012 period (A). Plot B shows a sub-population of the events displayed in A for ratios that with a value of between -20 and 20. Negative values were converted into positive values to aid in both the analysis and presentation of the data.

ventilation, the largest number of events (12) displayed a ratio between 2-10, with a mean of  $7.5 \pm 4.2$  and with a range between 2.5 and 16.0. The mean ratios found for NPP and ventilation represent 23% and 46% of the events identified, respectively, and are therefore suggestive of a common exchange ratio for these processes. However, at this level of analysis I cannot firmly conclude there is a common exchange ratio. The sample sizes of the events recorded are too small to deduce this (52 NPP events; 26 ventilation events). Furthermore, the differing timescales of exchange would suggest that a common ratio cannot be found for these events. Nonetheless, this analysis is suggestive of a common exchange ratio and so with further analyses, on a larger dataset, a common gas exchange ratio may indeed be found.

#### **4.5 Conceptual model of air-sea gas exchange**

The purpose of my conceptual model was to determine whether the carbon cycle events identified in the atmospheric  $O_2$  and  $CO_2$  observations could be reconciled with external datasets that also have the potential to characterise carbon cycle processes. Hence, NPP events, defined by an increase in APO over the event duration in the atmospheric observations, were compared to satellite estimates of NPP derived from the VGPM model of Behrenfeld and Falkowski (1997). Ventilation events, defined by a decrease in APO over the event duration, were compared to  $\Delta pO_2$  (derived from  $pO_2$  profiles in the region (Garcia et al., 2010)) as a result of mixing of deep- $O_2$ -depleted water masses with more oxygenated surface waters, which was defined by areas of ocean exhibiting a deep MLD estimated from Argo float profiles (Hosado et al., 2010). The conceptual model was only tested on events identified in the period 2006-2012. Before this period, a different set of meteorological input files had to be used in the Hysplit\_4 model back-trajectory analysis and would have therefore introduced an unnecessary error in my analysis. Consequently, 43 NPP events (83% of total) and 15 ventilation events (58% of total) were used in this section of the analysis.

##### *4.5.1 Origin of air masses arriving at Baring Head*

To display the results of the Hysplit\_4 air mass back-trajectory analysis, I divided the oceanic regions surrounding BHD into 4 sections: Tasman Sea, Pacific Ocean, South-West Southern Ocean and South-East Southern Ocean (Fig 4.11A). The majority of the air masses arriving at BHD originated from the Southern Ocean, accounting for 69.8% of NPP event trajectories and 86.7% of ventilation trajectories (Fig.4.11B). This confirms the ideal location for atmospheric sampling of the Southern Ocean that BHD provides. Furthermore, it is interesting to note that 18.7% of NPP trajectories originated from the Tasman Sea compared to ventilation trajectories (6.7%) and therefore highlights the importance of this region with respect to NPP (Baird et al., 2008), as discussed previously in Section 4.3.1.

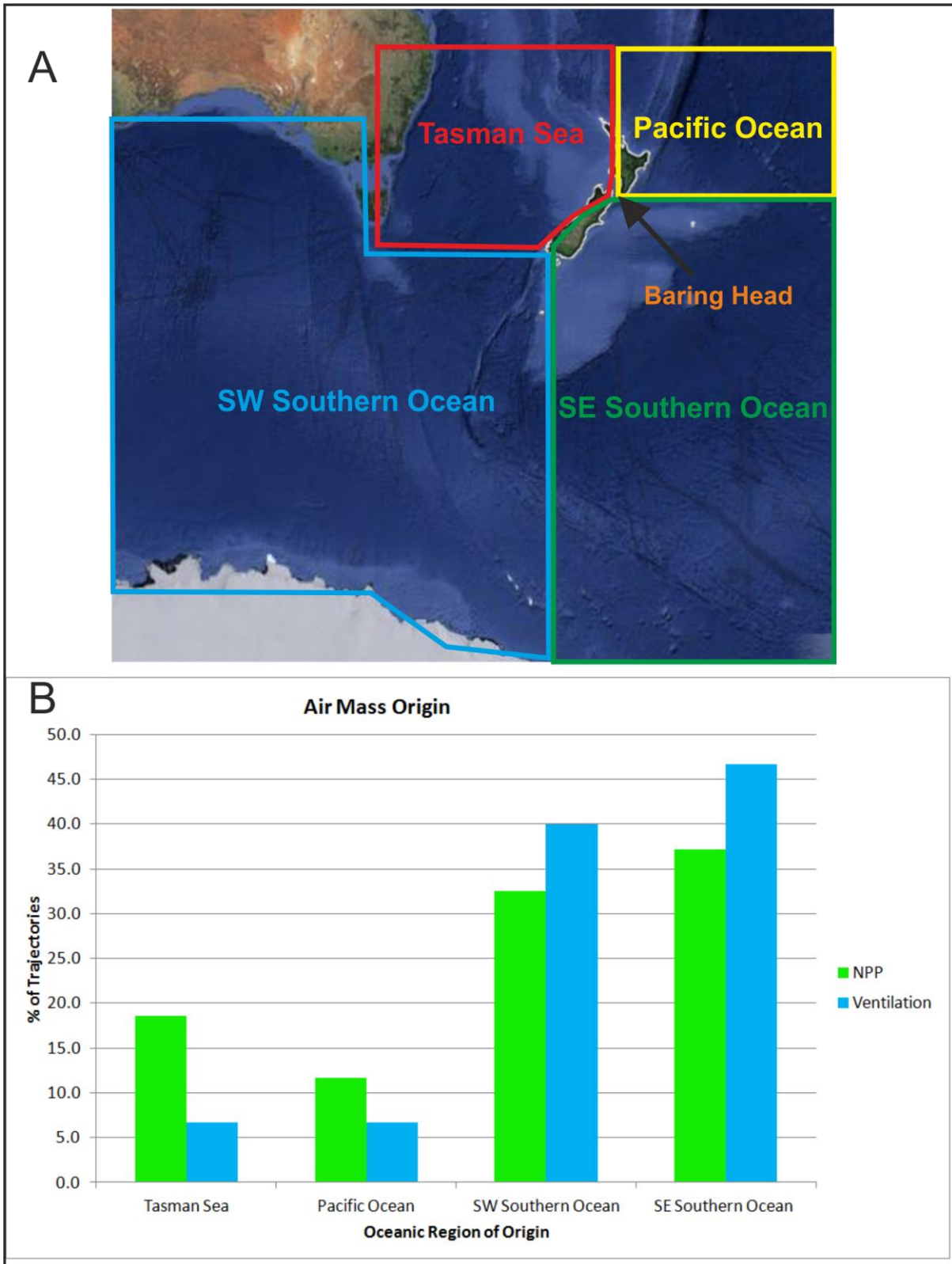


Figure 4.11 Results of the Hysplit\_4 air mass back trajectory analysis. Oceanic regions surrounding BHD were divided into 4 sections (described in text) (A). Air mass locations are displayed as a percentage of the total number of trajectories.

## 4.5.2 Testing the conceptual model

### 4.5.2.1 Net Primary Productivity (NPP)

The results of the conceptual model estimate of NPP, derived from the change in APO over the duration of each event, compared to the observed NPP derived from the satellite NPP estimate from the VGPM of Behrenfeld and Falkowski (1997) are displayed in Fig 4.12. My model overestimated the mean NPP by a least one order of magnitude. Despite this clear overestimation in the mean NPP, there should still be a positive correlation in the data, assuming that the change in APO over the duration of the event reflects the mean sea to air flux of O<sub>2</sub> integrated over the distance of ocean that the air mass back-trajectory covers (the wind fetch, L in Equation 1). That is to say, that a larger  $\Delta$ APO will result in a larger model NPP estimate which should correspond to a larger mean NPP derived from satellite observations. However, this does not appear to be the case as shown by the weak positive correlation ( $R^2 = 0.0011$ ) in Fig 4.12A. To see if this correlation coefficient could be improved, I removed 4 data points that displayed the highest overestimate of mean NPP, these were taken to be values  $>50000 \text{ mg C m}^{-2} \text{ yr}^{-1}$ . This only improved the correlation slightly however ( $R^2 = 0.0043$ ).

To examine the reliability of the model further, I compared the model NPP estimate to the maximum NPP values recorded by satellite observations within the oceanic region defined by the air-mass back trajectory analysis. Fig 4.12C-D show the results of this comparison for all of the data and with the 4 anomalous data points, defined above, removed. The correlation between the model and the maximum observed satellite NPP values is greatly improved, compared to that for mean, when all of the data are considered ( $R^2 = 0.35$ ) and further improved by removing the anomalous point ( $R^2 = 0.39$ ). This implies that the change in APO recorded over the duration of an event reflect the sea to air flux of O<sub>2</sub> only in the region of maximum NPP, rather than the mean O<sub>2</sub> flux estimated across the entire area of influence defined by the back-trajectory analysis. This interpretation is intuitive because in regions of high NPP the sea to air flux of O<sub>2</sub> will be greater than in regions of low NPP since the sea to air flux of O<sub>2</sub> is proportional to its dissolved concentration (Wanninkhof, 1992). This insight has important implications for the parameterization of the conceptual model. It implies the wind fetch (L) used in the flux calculation should be estimated only from where the air mass back trajectory intersects the region of maximum NPP, defined by the satellite observations, rather than those estimated over the entire length of the back-trajectory.

### 4.5.2.2 Ventilation

The results of the conceptual model estimate of  $\Delta pO_2$  compared to observed  $\Delta pO_2$  values derived from both  $pO_2$  depth profiles and MLD estimates are displayed in Fig 4.13. As mentioned, a total of 15 ventilation events were identified in the period 2006-2012. However, 3 of these events were discarded when the results of the back-trajectory analysis indicated that the air mass arriving at BHD

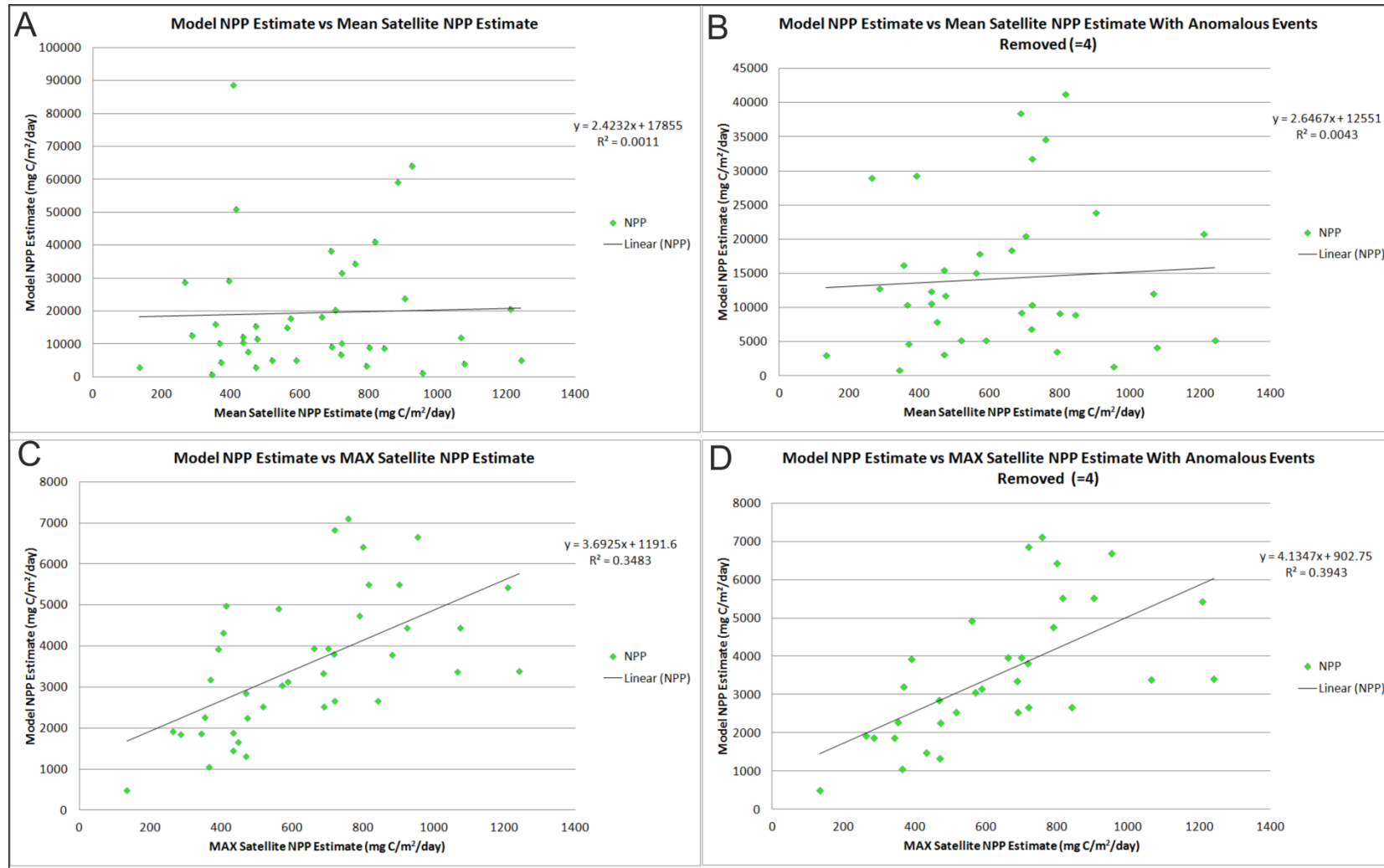


**Figure 4.12 Results of the conceptual model test for NPP events. Plot A displays the model NPP estimate compared to the mean satellite NPP estimate for all events in the 2006-2012 period. Plot B is the same as A, but with the 4 anomalous points removed (discussed in text). Plot C displays the model NPP estimate compared to the maximum satellite NPP estimate for all events whilst plot D displays the same as C but with the 4 anomalous data points removed.**

had not travelled over regions of ocean exhibiting deep mixed layers and hence won't represent ventilation processes. These events are not included in Fig 4.13.

My model consistently overestimates the observed decrease in  $pO_2$  due to ventilation (Fig. 4.13). Furthermore, no correlation can be found between the model  $\Delta pO_2$  estimate and the observed. If my model was parameterized correctly, then one would expect to see a positive correlation between the model estimates of  $\Delta pO_2$  and the observed since one would expect ventilation of deep- $O_2$ -deficient waters to drive a flux of  $O_2$  from the air to the sea and therefore a decrease in APO would be observed as the air mass arrives at BHD. There are two interpretations that could explain this lack of correlation within the data. Firstly, the data-set is too small, with only 12 events being used in the analysis. This is not a large enough dataset to assess correlations within the data. Conversely, it could be that the conceptual model is not parameterized correctly. The flux calculation used my model (Equation 1) assumes that the change in APO concentration is being influenced by air-sea gas exchange across the entire length of the trajectory, as it is in my NPP model. As with the NPP model, this is not a correct representation of what is actually happening in the real world. The air parcel recording the decline in APO will be more influenced by specific regions where ventilation is occurring, rather than being influenced by the entire area of ocean defined by the back-trajectory analysis. Therefore, as was discerned from analysis of the conceptual model for NPP, it seems more applicable to define the wind fetch (L) only over the region where the air-mass back-trajectory intersects the region of deep MLD. Further discussion on the limitations of my model is given in Section 4.5.4.

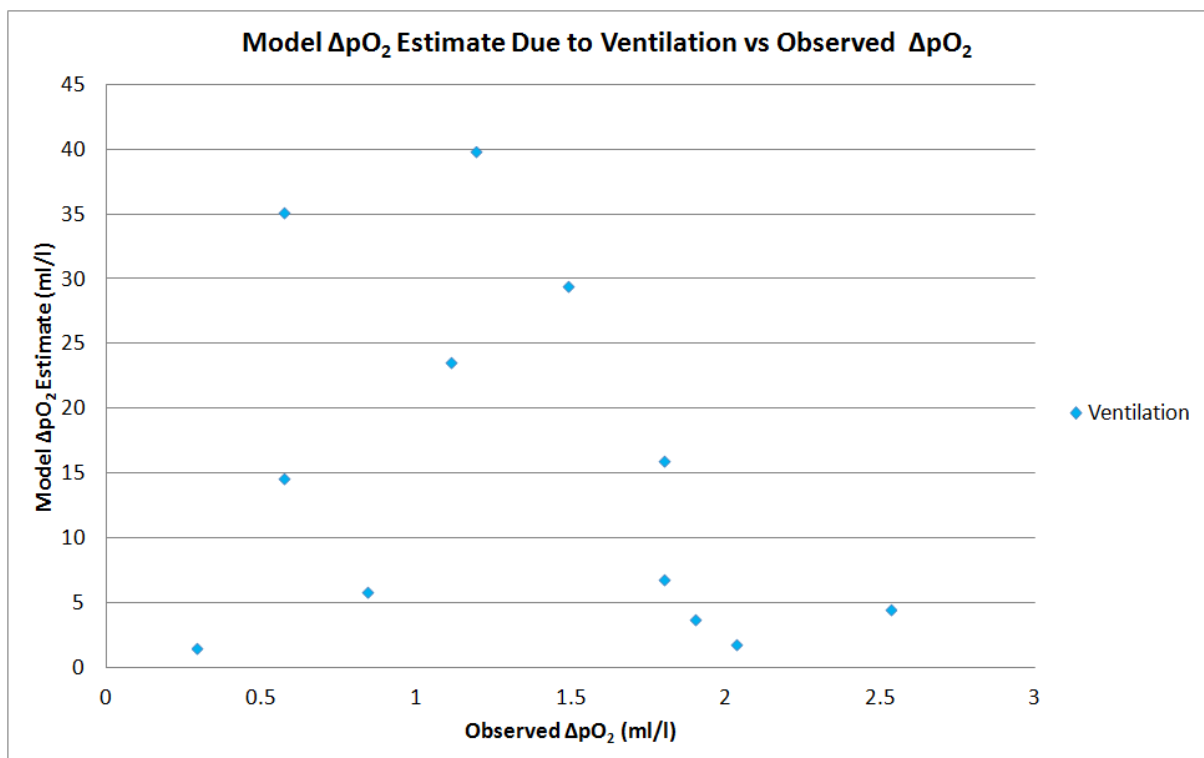


Figure 4.13. Displaying the model  $\Delta pO_2$  estimate from ventilation events compared to the observed  $\Delta pO_2$  between the surface and the MLD at the assumed region of ventilation.

### 4.5.3 Example NPP and ventilation events

The following section displays an example of a NPP and a ventilation event identified within my data analysis. I will provide evidence of how both events were identified, followed by the results of their air mass back-trajectory analysis displayed over a map projection of satellite NPP and MLD data. I will then show how the data fed into my conceptual model. As defined in Section 3.2.2, the conceptual model was based on the atmospheric ‘puff’ model derived by Jacob (1999) and used in a similar analysis to mine by Lueker et al., (2003), Thompson et al., (2007) and Yamagishi et al., (2008):

$$F = \frac{\rho_a \Delta Ch}{t[1 - \exp(-\frac{L}{ut})]} \quad \text{Equation 1 (for a definition of the variables refer back to Section 3.2.2)}$$

Fig 4.14 displays the NPP and ventilation events identified from atmospheric observations of APO. The NPP event begins at 12:42 on the 8<sup>th</sup> of November, 2010 and ends on the 11<sup>th</sup> at 10:37, giving an event duration of 69.9 hours. The magnitude of APO change is observed to be 100.9 per meg. The ventilation event begins at 10:20 on the 27<sup>th</sup> July 2006 and ends, on the same day at 23:47, giving an event duration of 13.5 hours. The 4-day air mass back-trajectory begins half way through the event duration and therefore begins at midnight on the 11<sup>th</sup> November for the NPP event, and at 5pm on the 27<sup>th</sup> July for the ventilation event. For the NPP event, the results of the back trajectory analysis were imported into an image of the 8-day average satellite NPP estimates spanning the period 3<sup>rd</sup>-11<sup>th</sup> November Fig 4.15A. For the ventilation event the results of the back trajectory analysis were imported into an image of the MLD for the period 24<sup>th</sup> July to 2<sup>nd</sup> August, derived from Argo float profile data (Fig 4.15B). As was defined in Section 3.2.2, I estimated the wind fetch, L, from the path length of the entire air mass back-trajectory. The wind fetch for the NPP event was therefore 4339km, whereas for the ventilation event it is 2775km.

For the NPP event identified, the flux of O<sub>2</sub> from the ocean to the atmosphere was 0.61 mol O<sub>2</sub> m<sup>-2</sup> day<sup>-1</sup>. Assuming this O<sub>2</sub> flux is entirely due to NPP, I convert the O<sub>2</sub> flux to a flux of carbon, assuming an exchange ratio (O<sub>2</sub>:C) for phytoplankton photosynthesis of 1.4 (Anderson, 1995). Hence, I derive a result of 0.43 mol C m<sup>-2</sup> day<sup>-1</sup>, which corresponds to a mass flux 5190 mg C m<sup>-2</sup> day<sup>-1</sup>. The mean satellite productivity estimate for the entire region of influence defined by the air mass back trajectory is 588±492 mg C m<sup>-2</sup> day<sup>-1</sup>, significantly below my model estimate. However, the maximum satellite productivity estimate derived from the region of influence is 3137 mg C m<sup>-2</sup> day<sup>-1</sup>, which agrees better with my model flux estimate and is the same order of magnitude. As was discussed in section 4.5.2, the maximum satellite NPP estimate is a better metric to compare my model to because sea-air fluxes will be more greatly influenced by regions of high NPP.

For the ventilation event identified, the flux of  $O_2$  from the atmosphere to the ocean is  $-1.6 \text{ mol } O_2 \text{ m}^{-2} \text{ day}^{-1}$ , the value is negative because the flux is into the ocean. However, unlike the NPP calculation, the ventilation  $O_2$  flux has to be converted to  $pO_2$ . The flux of a particular species into the ocean is related to its dissolved concentration by the gas-transfer velocity:

$$F = KC_w \quad \text{Equation 2 (see 3.2.2 for a definition of the variables).}$$

Using this equation, I obtain a  $pO_2$  for the ventilation event of  $-5.83 \text{ ml l}^{-1}$ . This value is assumed to represent the change in the surface water  $pO_2$  as a result of the upwelling and ventilation of a deep- $O_2$ -deficient water mass and is hence referred to as  $\Delta pO_2$ . This value was then directly compared to the difference between the  $pO_2$  at the surface and at the depth of the mixed layer through examining a cross-section of typical monthly  $pO_2$  profiles, derived from the World Ocean Atlas, 2009 (Garcia et al., 2010) across the region of influence (Fig 4.16). Fig 4.15B displays that the deepest MLD is at 657 decibars, equivalent to 670m, at a latitude of  $48.5^\circ\text{S}$ . These values are then used to estimate the  $\Delta pO_2$  in the  $pO_2$  plot shown in Fig 4.16. At the MLD,  $pO_2 = 5.51 \text{ ml l}^{-1}$ , whereas at the surface  $pO_2 = 6.35 \text{ ml l}^{-1}$ , corresponding to a  $\Delta pO_2$  of  $-0.84 \text{ ml l}^{-1}$ . As stated before, my model overestimates the  $\Delta pO_2$  by just under 1 order of magnitude.

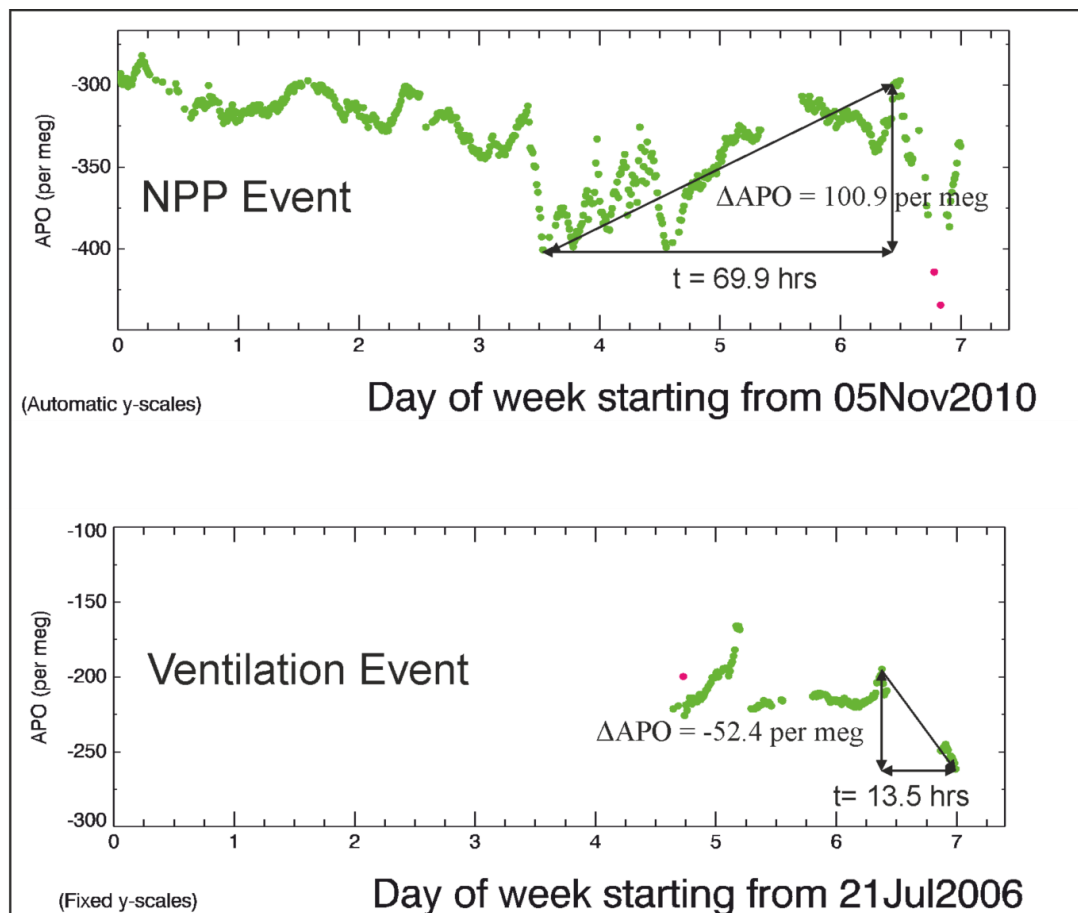


Figure 4.14. Identification of a NPP event during the week starting on the 5<sup>th</sup> November 2010 and of a ventilation event during the week starting on the 21<sup>st</sup> July 2006. The  $\Delta APO$  and  $t$  values used in the flux calculation are shown.

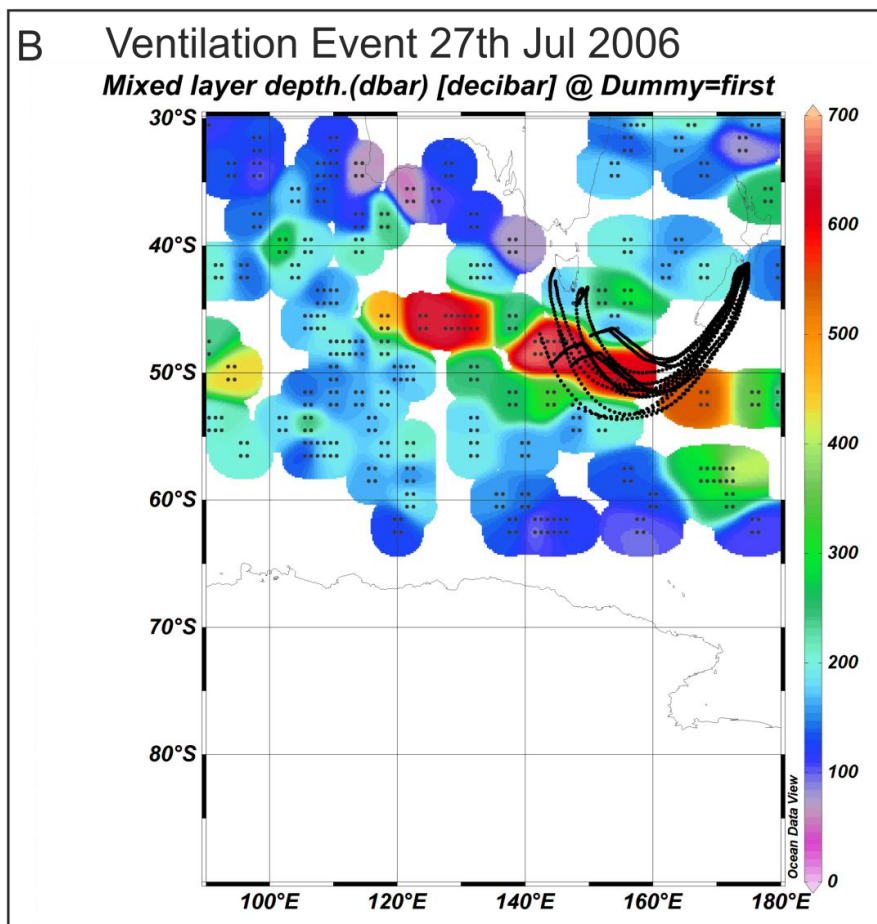
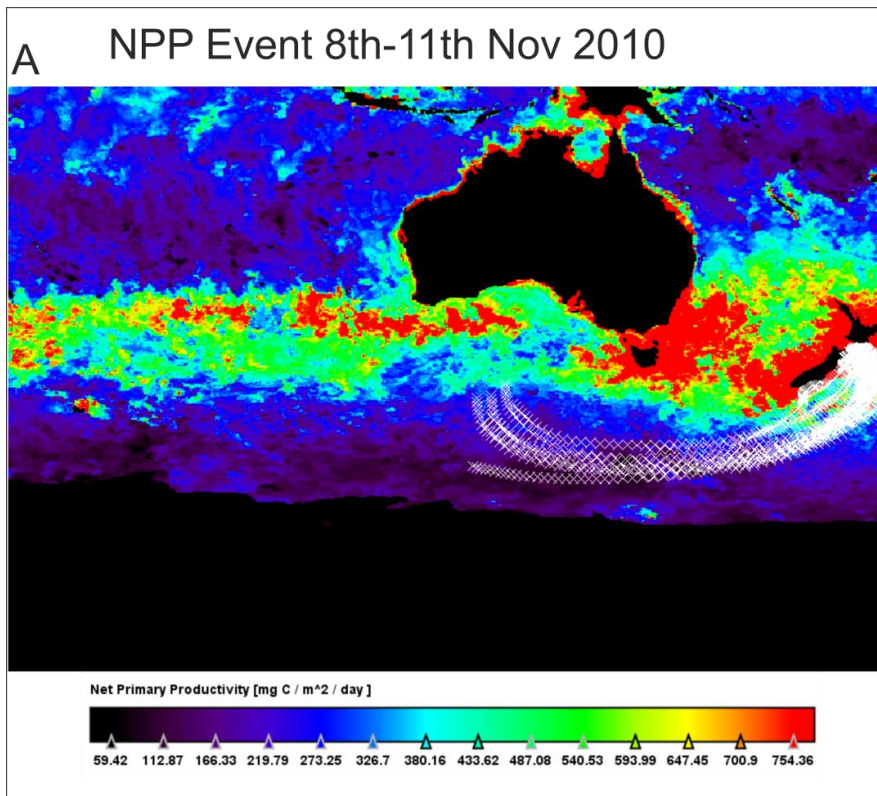


Figure 4.15. Results of the air-mass back trajectory analysis for the NPP event (A) and the ventilation event (B) overlaid onto a map projection of satellite NPP estimates ( $\text{mg C m}^{-2} \text{day}^{-1}$ ) (A) and of MLD estimates (dbar) (B).

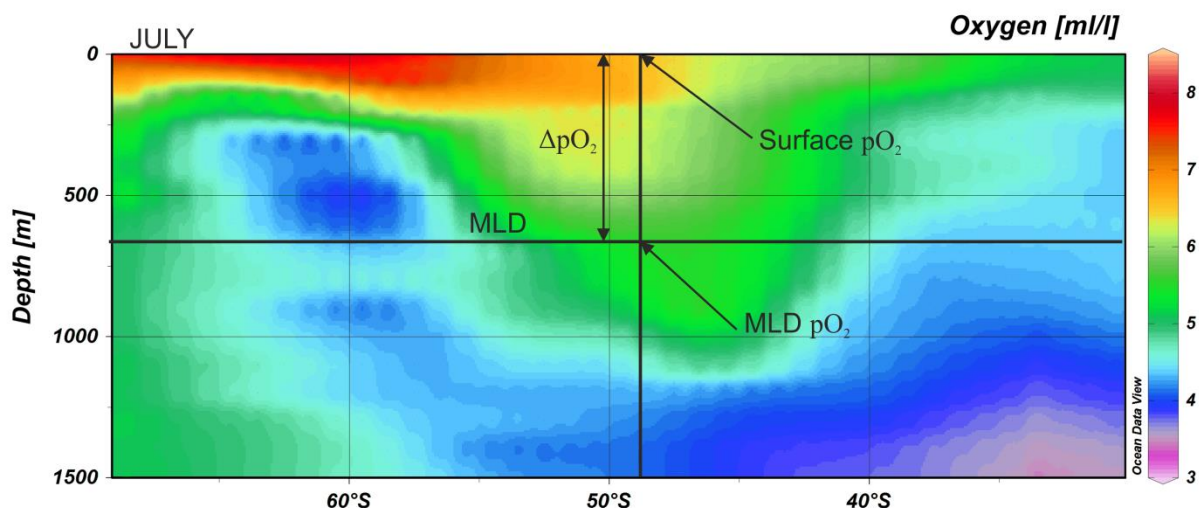


Figure 4.16.  $pO_2$  profile across a latitudinal section ( $30-70^\circ$ ) of the Southern Ocean at a longitude of  $158^\circ E$ . Displayed are the MLD estimated from Fig 4.15B for the ventilation event example.

#### 4.5.4 Limitations of the conceptual model.

It is important to consider the limitations of my conceptual model for air-sea gas exchange. The model is based on multiple variables that all have their own respective errors attached, including those associated with the Hysplit\_4 air-mass back-trajectory model of Draxler and Hess (1998), the VGPM model of Behrenfeld and Falkowski (1997) the MLD depth estimates from Argo float profile data (Hosoda et al., 2010) and the  $pO_2$  depth profiles of Garcia et al., (2010). In the follow up work to this project I plan on using a different suite of datasets to further test the reliability of the model. For example, the model may be improved by a better representation of the air mass origins such as those provided by the UK MET Office's Lagrangian particle Numerical Atmospheric Modelling Environment (NAME) dispersion model (Ryall and Marion, 1998). Furthermore, improved satellite estimates may be obtained from the improved carbon-based ocean productivity model of Behrenfeld (2005). Additionally, the monthly  $pO_2$  profiles of Garcia et al., (2010) are based on typical monthly depth profiles for the region and therefore do not represent the actual month and year that the ventilation events were identified in. It is possible that, if the correct time-series data of  $pO_2$  profiles are used then my model estimates may be more realistic.

As was discussed in Section 4.5.2, the parameterization of the wind fetch used in my analysis appears to be incorrect and may be better modelled by estimating the wind fetch only over the most productive regions for NPP events and for the region of deepest MLD for the ventilation events. Furthermore, there are substantial errors attached the Wanninkhof (1992) formulation relating fluxes of  $O_2$  to the  $pO_2$  concentration. This is because the gas-transfer velocity,  $K$ , is proportional to the average wind speed over the ocean and in regions of high wind speeds, such as the Southern Ocean, a small variation in the mean wind speed used results in a large variation in the  $K$  value derived (Ho et al., 2006).

## 5 Conclusions

The aim of this thesis project was to investigate the variability of atmospheric O<sub>2</sub> and CO<sub>2</sub> observations made at Baring Head, New Zealand, for the period 1999-2012, to make deductions on the temporal and spatial variability of the Southern Ocean carbon cycle. This was achieved through the identification of the carbon cycle processes of marine NPP and ventilation of deep CO<sub>2</sub>-rich, O<sub>2</sub> deficient water masses in the derived atmospheric APO observations. The events identified were then compared to either satellite NPP estimates or pO<sub>2</sub> estimates at the MLD by identifying oceanic regions of influence from the results of an air-mass back trajectory analysis of the air masses containing the APO variations. The results of this analysis were used to test the construction of a simple conceptual model of air-sea gas exchange. Furthermore, the atmospheric O<sub>2</sub>, CO<sub>2</sub> and APO for the study period were presented and an assessment of the global carbon sinks made. The inter-annual variability of APO was also assessed and compared to the SAM and ENSO climate indices.

### 5.1 Summary of key findings

- The average global oceanic and terrestrial carbon sinks were calculated to be 2.7 and 2.3 Pg C yr<sup>-1</sup>, respectively for the study period 1999-2012.
- The inter-annual variability of APO displayed no correlation with the SAM and ENSO climate indices. Further analyses are warranted however, given the sensitivity of my data to different curve fitting procedures, the choice of climate indices used and the potential for leads and lags within a possible correlation, which was not investigated.
- A total of 52 NPP events and 26 ventilation events were identified in the 1999-2012 period. The small sample size was discussed and considered when making deductions about the results.
- The inter-annual variability of the events identified is thought to represent uneven sampling of the data due to the variability of the wind direction at BHD, except in 2007 where the high number of recorded NPP events were presumed to reflect sampling of the productive Tasman Sea region and may therefore explain the increases in APO magnitude defined in the inter-annual variability of the species.
- The monthly variability of the events recorded was interpreted to represent the seasonal cycle of APO with a higher incidence of NPP events identified in the spring/summer months and a corresponding higher incidence of ventilation events identified in the autumn and winter months. The difference in the mean APO recorded by the events was found to be significantly different ( $P = 0.001$ ;  $<0.01$ ) between the autumn and spring months. This was interpreted to further represent the seasonal variation of APO, with a peak in APO in the early autumn as a result of high NPP during the summer months, and a trough in the early spring as a result of winter mixing and ventilation of CO<sub>2</sub> rich, O<sub>2</sub> poor water masses.

- The events identified were characterised by the rate of APO change over the duration of the event. NPP events showed  $\Delta\text{APO}/t$  values of  $\sim 2\text{-}3$  per meg  $\text{hr}^{-1}$  compared to ventilation events which typically displayed  $\Delta\text{APO}/t$  values of  $<1$  per meg  $\text{hr}^{-1}$ . This was interpreted to reflect the different spatial scales that these events occur over, whereby NPP is focused in the surface which would act to concentrate  $\text{O}_2$  in the surface layer, resulting in large  $\Delta\text{APO}/t$  values, whereas ventilation occurs over a much larger depth and so the relative  $\text{O}_2$  changes are suppressed.
- A common APO exchange ratio for the carbon cycle was suggested from the data, but not firmly ascertained due the paucity of sample data.
- The simple conceptual model of air-sea gas exchange was found to consistently overestimate both the NPP and magnitude of  $\text{O}_2$  change resulting from ventilation compared to satellite NPP and  $p\text{O}_2$  concentrations at the MLD. The limitations of the parameterizations used were therefore discussed and further analyses were proposed using different suites of data.

## 5.2 Suggestions for further research

This analysis has discussed the temporal and spatial variability of a relatively small set of identified carbon cycle processes. The events captured the monthly variability of APO very well, however they were not able to characterise the inter-annual variability well. As discussed, this study was perhaps limited by the small dataset. As such, I would suggest continuing this analysis on larger data-sets and from other regions surrounding the Southern Ocean to determine whether the inter-annual variability in APO can be better characterized. I plan on doing this on in-situ measurements at Amsterdam Island in the Southern Indian Ocean, which I intend to set up during my Ph.D, beginning in October, 2013 at the University of East Anglia. Furthermore, event identification was a very time consuming process and as such I intend to investigate the feasibility of writing a programming routine that can automatically select events of interest. Finally, my simple conceptual model may be better represented by alternative suites of data, such as by using the U.K Met office's NAME model. I therefore intend to investigate this further in my Ph.D.

## 6 Reference List

- Anderson, Laurence A. 1995. "On the Hydrogen and Oxygen Content of Marine Phytoplankton." *Deep Sea Research Part I: Oceanographic Research Papers* 42 (9): 1675–1680.
- Baird, Mark E., Patrick G. Timko, Jason H. Middleton, Thomas J. Mullaney, Deborah R. Cox, and Iain M. Suthers. 2008. "Biological Properties Across the Tasman Front Off Southeast Australia." *Deep Sea Research Part I: Oceanographic Research Papers* 55 (11) (November): 1438–1455. doi:10.1016/j.dsr.2008.06.011
- Balkanski, Yves Patrick Monfray Mark Battle Martin Heimann. 1999 "Ocean primary production derived from satellite data: An evaluation with atmospheric oxygen measurements. *Global Biogeochemical Cycles* Volume 13, Issue 2, pages 257–271, June 1999
- Battle, Mark, Sara Mikaloff Fletcher, Michael L. Bender, Ralph F. Keeling, Andrew C. Manning, Nicolas Gruber, Pieter P. Tans, et al. 2006. "Atmospheric Potential Oxygen: New Observations and Their Implications for Some Atmospheric and Oceanic Models: APO MEASUREMENTS AND MODELS." *Global Biogeochemical Cycles* 20 (1) (March): n/a–n/a. doi:10.1029/2005GB002534.
- Behrenfeld, Michael J., and Paul G. Falkowski. 1997. "Photosynthetic Rates Derived from Satellite-based Chlorophyll Concentration." *Limnology and Oceanography* 42 (1): 1–20.
- Bender, M. L. and Battle, M. O. (1999), "Carbon cycle studies based on the distribution of O<sub>2</sub> in air". *Tellus B*, 51: 165–169. doi: 10.1034/j.1600-0889.1999.t01-1-00004.x
- Bender, M., T. Ellis, P. Tans, R. Francey, and D. Lowe (1996), "Variability in the O<sub>2</sub>/N<sub>2</sub> ratio of southern hemisphere air, 1991–1994: Implications for the carbon cycle", *Global Biogeochem. Cycles*, 10(1), 9–21, doi:10.1029/95GB03295
- Berner, Robert A. 1998. "The Carbon Cycle and Carbon Dioxide over Phanerozoic Time: The Role of Land Plants." *Philosophical Transactions of the Royal Society of London. Series B: Biological Sciences* 353 (1365): 75–82.
- Boden Tom Andres Bob 2013 Global CO<sub>2</sub> Emissions from Fossil-Fuel Burning, Cement Manufacture, and Gas Flaring: 1751-2010 Carbon Dioxide Information Analysis Center, Oak Ridge National Laboratory Oak Ridge, Tennessee 37831-6290 US

Broecker, Wallace S. Peng, Tsung-hung Beng Zonghong “Tracers in the sea” Lamont-Doherty Geological Observatory, Columbia University, 1982

Doney, Scott C., Victoria J. Fabry, Richard A. Feely, and Joan A. Kleypas. 2009. “Ocean Acidification: The Other CO<sub>2</sub> Problem.” *Annual Review of Marine Science* 1 (1) (January): 169–192. doi:10.1146/annurev.marine.010908.163834.

Dong, Shenfu, Janet Sprintall, Sarah T. Gille, and Lynne Talley. 2008. “Southern Ocean Mixed-layer Depth from Argo Float Profiles.” *Journal of Geophysical Research* 113 (C6) (June 13). doi:10.1029/2006JC004051. <http://doi.wiley.com/10.1029/2006JC004051>.

Draxler, Roland R., and G. D. Hess. 1998. “An Overview of the HYSPLIT\_4 Modelling System for Trajectories.” *Australian Meteorological Magazine* 47 (4). <ftp://129.82.109.126/Braun/Aviation%20Weather/Volcanoes/VA%20Modeling/OverviewHYSPLIT4.pdf>.

Garcia, H. E., R. A. Locarnini, T. P. Boyer, and J. I. Antonov, 2010. World Ocean Atlas 2009 Volume 3: Dissolved Oxygen, Apparent Oxygen Utilization, and Oxygen Saturation. S. Levitus, Ed., NOAA Atlas NESDIS 70, U.S. Government Printing Office, Washington, D.C., 344 pp

Gloor, M., J. L. Sarmiento, and N. Gruber. 2010. “What Can Be Learned About Carbon Cycle Climate Feedbacks from the CO<sub>2</sub>; Airborne Fraction?” *Atmospheric Chemistry and Physics* 10 (16) (August 20): 7739–7751. doi:10.5194/acp-10-7739-2010.

Gruber, N., Gloor, M., Fan, S.-M., & Sarmiento, J. L. (2001). “Air-sea flux of oxygen estimated from bulk data: Implications for the marine and atmospheric oxygen cycles”. *Global Biogeochemical Cycles*, 15(4), 783-803

Hamme, Roberta C., and Ralph F. Keeling. 2008. “Ocean Ventilation as a Driver of Interannual Variability in Atmospheric Potential Oxygen.” *Tellus B* 60 (5) (November): 706–717. doi:10.1111/j.1600-0889.2008.00376.x

Hansen, J., Mki. Sato, and R. Ruedy, 1997:” Radiative forcing and climate response”. *J. Geophys. Res.*, 102, 6831-6864, doi:10.1029/96JD03436

IPCC 2007. Solomon, S.,D. Qin, M. Manning, Z. Chen, M. Marquis, K.B. Averyt, M. Tignor and H.L. Miller (eds.). *Climate Change 2007: The Physical Science Basis. Contribution of Working Group I to the Fourth Assessment Report of the Intergovernmental Panel on Climate Change* Cambridge University Press, Cambridge, United Kingdom and New York, NY, USA

Keeling, R 1988 “Measuring correlations between atmospheric oxygen and carbon dioxide mole fractions: A preliminary study in urban air”. *Journal of Atmospheric Chemistry* 0167-7764 V 7 /BF00048044

Keeling, Ralph F and Shertz, Stephen R. 1992. “Seasonal and interannual variations in atmospheric oxygen and implications for the global carbon cycle” *Nature*. V.358. Is 6389 <http://dx.doi.org/10.1038/358723a0>

Keeling et al. 1996 Global and Hemispheric CO<sub>2</sub> Sinks Deduced from Changes in Atmospheric O<sub>2</sub> Concentrations. *Nature* 381, 218-221 (16 May 1996) | doi:10.1038/381218a0;

Keeling, R. F., R. P. Najjar, M. L. Bender, and P. P. Tans (1993), What atmospheric oxygen measurements can tell us about the global carbon cycle, *Global Biogeochem. Cycles*, 7(1), 37–67, doi:[10.1029/92GB02733](https://doi.org/10.1029/92GB02733).

Law, R. M., R. J. Matear, and R. J. Francey. 2008. “Comment on ‘Saturation of the Southern Ocean CO<sub>2</sub> Sink Due to Recent Climate Change’.” *Science* 319 (5863) (February 1): 570a–570a. doi:10.1126/science.1149077.

Le Quere, C., C. Rodenbeck, E. T. Buitenhuis, T. J. Conway, R. Langenfelds, A. Gomez, C. Labuschagne, et al. 2007. “Saturation of the Southern Ocean CO<sub>2</sub> Sink Due to Recent Climate Change.” *Science* 316 (5832) (June 22): 1735–1738. doi:10.1126/science.1136188.

———. 2008. “Response to Comments on ‘Saturation of the Southern Ocean CO<sub>2</sub> Sink Due to Recent Climate Change’.” *Science* 319 (5863) (February 1): 570c–570c. doi:10.1126/science.1147315.

Le Quéré, Corinne, Michael R. Raupach, Josep G. Canadell, Gregg Marland et al., Corinne Le Quéré et al., Corinne Le Quéré et al., Michael R. Raupach, et al. 2009. “Trends in the Sources and Sinks of Carbon Dioxide.” *Nature Geoscience* 2 (12) (November 17): 831–836. doi:10.1038/ngeo689.

Lenton, Andrew, and Richard J. Matear. 2007. “Role of the Southern Annular Mode (SAM) in Southern Ocean CO<sub>2</sub> Uptake: SAM AND SOUTHERN OCEAN CO<sub>2</sub> UPTAKE.” *Global Biogeochemical Cycles* 21 (2) (June): n/a–n/a. doi:10.1029/2006GB002714.

- Lovenduski, Nicole S., Nicolas Gruber, and Scott C. Doney. 2008. "Toward a Mechanistic Understanding of the Decadal Trends in the Southern Ocean Carbon Sink: SOUTHERN OCEAN CO<sub>2</sub> FLUX TRENDS." *Global Biogeochemical Cycles* 22 (3) (September): n/a–n/a. doi:10.1029/2007GB003139.
- Lovenduski, Nicole S., Nicolas Gruber, Scott C. Doney, and Ivan D. Lima. 2007. "Enhanced CO<sub>2</sub> Outgassing in the Southern Ocean from a Positive Phase of the Southern Annular Mode" *Global Biogeochemical Cycles* 21 (2) (June): doi:10.1029/2006GB002900.
- Lueker, Timothy J. 2003. "Coastal Upwelling Air-sea Fluxes Revealed in Atmospheric Observations of O<sub>2</sub>/N<sub>2</sub>, CO<sub>2</sub> and N<sub>2</sub>O." *Geophysical Research Letters* 30 (6). doi:10.1029/2002GL016615. <http://doi.wiley.com/10.1029/2002GL016615>.
- Manning, Andrew C., and Ralph F. Keeling. 2006. "Global Oceanic and Land Biotic Carbon Sinks from the Scripps Atmospheric Oxygen Flask Sampling Network." *Tellus B* 58 (2): 95–116.
- Manning, Andrew 2001. "Temporal variability of atmospheric oxygen from both continuous measurements and a flask sampling network: Tools for studying the global carbon cycle. Ph.D Thesis
- Marshall, Gareth J. 2003. "Trends in the Southern Annular Mode from Observations and Reanalyses." *Journal of Climate* 16 (24): 4134–4143.
- Metzl, N., C. Brunet, A. Jabaud-Jan, A. Poisson, and B. Schauer. 2006. "Summer and Winter Air–sea CO<sub>2</sub> Fluxes in the Southern Ocean." *Deep Sea Research Part I: Oceanographic Research Papers* 53 (9) (September): 1548–1563. doi:10.1016/j.dsr.2006.07.006.
- Mikaloff Fletcher, S. E., N. Gruber, A. R. Jacobson, M. Gloor, S. C. Doney, S. Dutkiewicz, M. Gerber, et al. 2007. "Inverse Estimates of the Oceanic Sources and Sinks of Natural CO<sub>2</sub> and the Implied Oceanic Carbon Transport: NATURAL AIR-SEA FLUXES OF CO<sub>2</sub>." *Global Biogeochemical Cycles* 21 (1) (March): n/a–n/a. doi:10.1029/2006GB002751.
- Nevison, C. D., R. F. Keeling, M. Kahru, M. Manizza, B. G. Mitchell, and N. Cassar. 2012. "Estimating Net Community Production in the Southern Ocean Based on Atmospheric Potential Oxygen and Satellite Ocean Color Data: APO AND OCEAN COLOR." *Global Biogeochemical Cycles* 26 (1) (March): n/a–n/a. doi:10.1029/2011GB004040.
- Reinsch, Christian H. 1967. "Smoothing by Spline Functions." *Numerische Mathematik* 10 (3): 177–183.

- Rintoul, Stephen R. 2011. "The Southern Ocean in the Earth System." *Proceedings and Other Publications*. <http://smithsonianrex.si.edu/sisp/index.php/pop/article/view/410>.
- Peters, Glen Marland, Gregg Le Quere, Corinne Boden, Thomas Canadell, Josep G. Raupach, Michael R. 2012. "Rapid growth in CO<sub>2</sub> emissions after the 2008-2009 global financial crisis" *Nature Clim. Change* V1.2 Is 1 1758-678X <http://dx.doi.org/10.1>
- Pickers, Penelope. 2012. Investigating bias in the application of three curve fitting programs to atmospheric time series. MSc Thesis. University of East Anglia.
- Roy, T.; Rayner, P. J.; Matear, R. J.; Francey, R. J. 2003 "Southern Hemisphere Ocean Co<sub>2</sub> Uptake: Reconciling Atmospheric and Oceanic Estimates." *Tellus* 701-710; 55B 2
- Sabine, C. L. 2004. "The Oceanic Sink for Anthropogenic CO<sub>2</sub>." *Science* 305 (5682) (July 16): 367–371. doi:10.1126/science.1097403.
- Sallée, Jean-Baptiste, Richard J. Matear, Stephen R. Rintoul, and Andrew Lenton. 2012. "Localized Subduction of Anthropogenic Carbon Dioxide in the Southern Hemisphere Oceans." *Nature Geoscience* 5 (8) (July 29): 579–584. doi:10.1038/ngeo1523.
- Shindell, Drew T. 2004. "Southern Hemisphere Climate Response to Ozone Changes and Greenhouse Gas Increases." *Geophysical Research Letters* 31 (18). doi:10.1029/2004GL020724. <http://doi.wiley.com/10.1029/2004GL020724>.
- Siegenthaler, U. 2005. "Stable Carbon Cycle-Climate Relationship During the Late Pleistocene." *Science* 310 (5752) (November 25): 1313–1317. doi:10.1126/science.1120130.
- Solomon, S., D. Qin, M. Manning, Z. Chen, M. Marquis, K.B. Averyt, M. Tignor and H.L. Miller (eds.). *Climate Change 2007: The Physical Science Basis. Contribution of Working Group I to the Fourth Assessment Report of the Intergovernmental Panel on Climate Change* Cambridge University Press, Cambridge, United Kingdom and New York, NY, USA..
- Stephens, B. B., G. W. Brailsford, A. J. Gomez, K. Riedel, S. E. Mikaloff Fletcher, S. Nichol, and M. Manning. 2013. "Analysis of a 39-year Continuous Atmospheric CO<sub>2</sub>; Record from Baring Head, New Zealand." *Biogeosciences* 10 (4) (April 23): 2683–2697. doi:10.5194/bg-10-2683-2013.

- Stephens, B. B., R. F. Keeling, M. Heimann, K. D. Six, R. Murnane, and K. Caldeira (1998), Testing global ocean carbon cycle models using measurements of atmospheric O<sub>2</sub> and CO<sub>2</sub> concentration, *Global Biogeochem. Cycles*, 12(2), 213–230, doi:[10.1029/97GB03500](https://doi.org/10.1029/97GB03500).
- Takahashi, Taro, Stewart C. Sutherland, Richard A. Feely, and Rik Wanninkhof. 2006a. “Decadal Change of the Surface Water pCO<sub>2</sub> in the North Pacific: A Synthesis of 35 Years of Observations.” *Journal of Geophysical Research* 111 (C7). doi:[10.1029/2005JC003074](https://doi.org/10.1029/2005JC003074). <http://doi.wiley.com/10.1029/2005JC003074>.
- . 2006b. “Decadal Change of the Surface Water pCO<sub>2</sub> in the North Pacific: A Synthesis of 35 Years of Observations.” *Journal of Geophysical Research* 111 (C7). doi:[10.1029/2005JC003074](https://doi.org/10.1029/2005JC003074). <http://doi.wiley.com/10.1029/2005JC003074>.
- Talley, Lynned D. 2013. “Closure of the Global Overturning Circulation Trough the Indian, Pacific, and Southern Oceans.” *Oceanography* 26 (1): 70.
- Thompson, D.W.J. and Solomon, S. 2002. Interpretation of recent Southern Hemisphere climate change. *Science* 296: 895-899
- Thompson, Rona L., Andrew C. Manning, David C. Lowe, and David C. Weatherburn. 2007. “A Ship-based Methodology for High Precision Atmospheric Oxygen Measurements and Its Application in the Southern Ocean Region.” *Tellus B* 59 (4) (September): 643–653. doi:[10.1111/j.1600-0889.2007.00292.x](https://doi.org/10.1111/j.1600-0889.2007.00292.x).
- Tohjima, Y. 2005. “First Measurements of the Latitudinal Atmospheric O<sub>2</sub> and CO<sub>2</sub> Distributions Across the Western Pacific.” *Geophysical Research Letters* 32 (17). doi:[10.1029/2005GL023311](https://doi.org/10.1029/2005GL023311). <http://doi.wiley.com/10.1029/2005GL023311>.
- Wanninkhof, Rik. 1992. “Relationship Between Wind Speed and Gas Exchange over the Ocean.” *Journal of Geophysical Research: Oceans (1978–2012)* 97 (C5): 7373–7382.
- Watson, A. J., U. Schuster, D. C. E. Bakker, N. R. Bates, A. Corbiere, M. Gonzalez-Davila, T. Friedrich, et al. 2009. “Tracking the Variable North Atlantic Sink for Atmospheric CO<sub>2</sub>.” *Science* 326 (5958) (December 3): 1391–1393. doi:[10.1126/science.1177394](https://doi.org/10.1126/science.1177394).
- Watson, Andrew J., and Alberto C. Naveira Garabato. 2006. “The Role of Southern Ocean Mixing and Upwelling in Glacial-interglacial Atmospheric CO<sub>2</sub> Change.” *Tellus B* 58 (1) (February): 73–87. doi:[10.1111/j.1600-0889.2005.00167.x](https://doi.org/10.1111/j.1600-0889.2005.00167.x).

- Wunsch, Carl, and Patrick Heimbach. 2006. "Estimated Decadal Changes in the North Atlantic Meridional Overturning Circulation and Heat Flux 1993-2004." *Journal of Physical Oceanography* 36 (11): 2012–2024.
- Yamagishi, H., Y. Tohjima, H. Mukai, and K. Sasaoka. 2008. "Detection of Regional Scale Sea-to-air Oxygen Emission Related to Spring Bloom Near Japan by Using In-situ Measurements of the Atmospheric Oxygen/nitrogen Ratio." *Atmospheric Chemistry and Physics* 8 (12): 3325–3335.
- Zachos, J. 2001. "Trends, Rhythms, and Aberrations in Global Climate 65 Ma to Present." *Science* 292 (5517) (April 27): 686–693. doi:10.1126/science.1059412.
- Zickfeld, K., J. C. Fyfe, M. Eby, and A. J. Weaver. 2008. "Comment on 'Saturation of the Southern Ocean CO<sub>2</sub> Sink Due to Recent Climate Change'." *Science* 319 (5863) (February 1): 570b–570b. doi:10.1126/science.1146886.

## 7 Appendices

The Appendices were chosen not to be included in the presentation of my thesis. What was intended for the appendices included all of the data produced within the project. This includes all satellite imagery data, mixed layer depth data, dissolved oxygen data, back-trajectory data and the records atmospheric observations. This represents 10GB of data and would therefore not be appropriate to attach to this thesis. Therefore if you require any of the datasets used, I can bring them to you on a portable hard drive, or if you require specific sets of data I can transfer them through Dropbox to you. Please email me at [stbarningham@gmail.com](mailto:stbarningham@gmail.com) if you wish to arrange this.



